Polymer Matrix Composites, Chapter 13, R. Talreja and J-A. Månson, eds., in press (2000) Author prepared preprint
Volume 2 of *Comprehensive Composite Materials*, A. Kelly and C. Zweben, eds., Elsevier Science

2.13 Matrix Microcracking in Composites

John A. Nairn
University of Utah, Salt Lake City, Utah, USA

2.13.1 INTRODUCTION

The first form of damage in laminates is usually matrix microcracks [1], which are intralaminar or ply cracks that traverse the thickness of the ply and run parallel to the fibers in that ply. The most common observation of microcracking is cracking in 90° plies during axial loading in the 0° direction. These microcracks are transverse to the loading direction and thus sometimes called transverse cracks. The terms matrix microcracks, microcracks, intralaminar cracks, ply cracks, and transverse cracks are found often in the composite literature. They usually refer to the same cracking phenomenon and they are the subject of this chapter.

By any name, microcracks can be observed during tensile loading, during fatigue loading, during changes in temperature, and during thermocycling. Microcracks can form in any plies, but they form predominantly in plies off-axis to loading directions. The immediate effect of microcracks is to cause a degradation in the thermomechanical properties of the laminate including changes in all effective moduli, Poisson ratios, and thermal expansion coefficients. If a given design can not tolerate microcrack-induced degradation in properties, then the formation of microcracks constitutes failure of the design. A secondary effect of microcracks is that they nucleate other forms of damage. For example, microcracks can induce delaminations, cause fiber

breaks, or provide pathways for entry of corrosive liquids. Such damage modes may subsequently lead to laminate failure. The processes by which microcracks form, the effects they have on laminate properties, and their role in nucleating new forms of damage are all important problems in the analysis of failure of composite laminates.

This chapter will begin by summarizing experimental observations about microcracking. Microcracking studies began in the 1970's with observations of the initiation of microcracking [2]. Since then there have been numerous papers on the microcracking process under a variety of loading and environmental conditions. A major interest in studying microcracking is to be able to predict the microcracking process and to be able to design laminates that are resistant to microcracking. Early attempts at modeling microcracking assumed microcracks formed when the stress in the off-axis plies reaches the transverse strength of the ply material. Numerous experimental observations show that such strength models do a poor job of correlating the now large body of experimental observations. This chapter, will present instead methods for analyzing microcracking based on fracture mechanics or energy balance methods. In these methods, the next microcrack is assumed to form when the total energy released by the formation of the microcrack reaches a critical value denoted here as the material microcracking fracture toughness, G_{mc}. This chapter will focus on microcracking in 90° plies with the predominant loading direction normal to those cracking plies. All principles discussed, however, are adaptable to analysis of microcracking in more general laminates with more general loading conditions.

There are many applications of the energy analysis of microcracking. Perhaps most important, the fracture mechanics methods can be used to analyze experimental results to determine G_{mc} for a given type of composite material. This material property can be used to rank materials according to their resistance to microcracking. Because microcracks are the first form of failure in many laminates, G_{mc} is a sensitive probe of laminate failure properties. By measuring changes in G_{mc} in various aging environments, it is possible to study degradation of laminates and make predictions about durability. Another advantage of the energy analysis is that it can be extended to explain microcracking during fatigue loading either by cyclic mechanical loads or cyclic changes in temperature. The energy analysis of microcracking during fatigue provides more tools for assessing the resistance of a given type of composite material to the formation of fatigue-induced microcracks.

Another important area is the effect of microcracks on the thermomechanical properties of microcracked laminates. It might be important for a designer to know the degradation in properties caused by microcracks to be able to assess the level of microcracking that can be tolerated before the structure has failed. As discussed in this chapter, the energy analysis of microcracking can be based rigorously in terms of effective laminate properties. Thus, once the energy analysis is completed, most information about degradation of thermomechanical properties is known as well. This chapter will outline the latest results on effective thermomechanical properties of laminates with microcracks.

2.13.2 EXPERIMENTAL OBSERVATIONS

2.13.2.1 Initiation of Microcracking

The first form of damage in laminates having 90° plies is often microcracking in those plies. The formation of the first crack is the initiation of microcracking. Garrett, Bailey, *et al.* [2–8] did a series of microcracking experiments, including observations of microcrack initiation on $[0/90]_s$ laminates made from glass-reinforced polyester [2, 3] and from glass-reinforced epoxy [4–8]. By working with home-made $[0/90]_s$ laminates, they continuously varied the thickness of the 90° plies from less than 0.1 mm to 4.0 mm while keeping the thickness of the supporting 0° plies constant at 0.5 mm [4]. Their results, replotted in Fig. 1, show that there is a significant effect of 90° ply thickness on the strain to microcrack initiation. As the thickness of the 90° plies decreases and becomes less than the 0.5 mm thickness of the 0° plies, the strain to microcrack initiation increases.

Besides the increase in strain to initiate microcracking, the thickness of the 90° plies affects the entire microcracking process. For 90° plies greater than 0.5 mm thick (or equal to or greater than the 0° ply thickness), microcracks form as instantaneous fracture events. On the experimental time-scale, the microcrack initiates and propagates over the entire cross-sectional area of the 90° plies instantaneously. For thicknesses

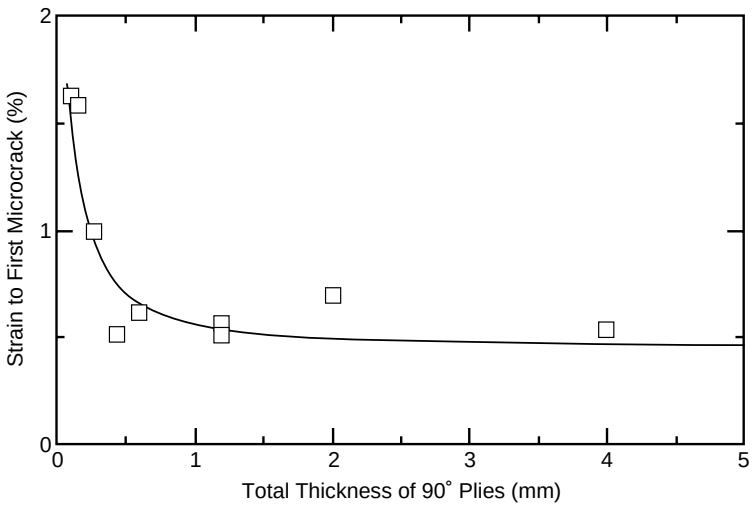

Figure 1 The strain to initiate microcracking in glass-reinforced $[0/90]_s$ laminates as a function of the total thickness of the 90° plies. The 0° plies each have a constant thickness of 0.5 mm. The data is from Ref. [2].

between 0.1 mm and 0.4 mm, individual microcracks can sometimes be observed to initiate on the free edges and propagate across the width of the laminate. For thicknesses less than 0.1 mm, the microcracks are suppressed entirely and the laminate fails before initiation of microcracking.

A common method for designing with composites to avoid failures is first-ply failure theory. In first-ply failure theory, it is assumed that the first ply cracks or fails when the strain in those plies reaches the strain to failure of those plies [9]. Furthermore, it is usually assumed that the ply failure strain can be determined from experiments on isolated unidirectional laminates. The results are not good if one tries to use first-ply failure theory to predict microcrack initiation. In laminated plate theory of $[0/90]_s$ laminates under tensile loading, the strains in the 0° and 90° plies, including residual strains due to thermal stresses, can be easily calculated and they are nearly independent of ply thicknesses. Thus, first-ply failure theory predicts that the strain to initiate microcracking will be independent of ply thickness; this prediction contradicts all experimental observation of microcrack initiation. Attempts to use more *sophisticated* ply-failure criteria [10] to account for multi-axial stresses when the plies are in a laminate are no help; all components of stress are nearly independent of ply thickness and thus all strength-based models predict microcrack initiation to be independent of ply thickness. No strength-based, first-ply failure model can be used to predict microcrack initiation unless the ply failure properties are treated as *in situ* properties that depend on laminate structure. Modification of first-ply failure theory to use *in situ* properties severely limits it predictive capabilities. The energy methods discussed in this chapter can predict microcracking properties without resorting to the use of *in situ* failure properties.

It is interesting to consider a design case-study using laminated plate theory software with failure analysis by first-ply failure theory and a quadratic failure criterion [10] that attempts to account for multi-axial stress state effects. Imagine seeking to design a $[0_n/90_m]_s$ laminate with the goal of preventing all microcracks in the 90° plies. Although axial strain in the 90° plies is independent of thickness, the quadratic failure criterion predicts that the axial strain required to cause first-ply failure increases slightly as the 90° plies get thicker. The optimal design based on such a strength-based theory is thus to make the 90° plies as *thick* as possible. In contrast, the correct optimal design, based on experimental results (see Fig. 1), is to make the 90° plies as *thin* as possible.

Similar microcrack initiation experiments with similar results have been done on carbon fiber/epoxy laminates [5, 6, 11]. The strain to initiate microcracking increases as the thickness of the 90° plies decreases. Flaggs and Kural [11] tested a wide range of carbon-epoxy laminates with 90° plies. Using laminated plate theory, they calculated the strain in the 90° plies at the onset of cracking (the *in situ* failure strain) and compared it to the transverse strain to failure of the corresponding unidirectional plies. They found that the *in situ* failure strain is always larger than the transverse failure strain of the ply material. Clearly, first-ply failure models based on transverse failure strain of the ply material are inadequate for predicting onset of

microcracking in laminates.

Microcracks in carbon fiber/epoxy laminates always formed instantaneously across the entire cross sectional area of the 90° plies [5, 6, 11]. This observation contrasts with the glass fiber/epoxy results where microcracking becomes partially or totally suppressed as the 90° plies get thin. Partial suppression of microcracks in glass fiber/epoxy laminates, however, requires making the 90° plies thinner than the 0° plies; total suppression requires making them five times thinner. None of the experiments on carbon fiber/epoxy laminates, however, have tested specimens with such thin 90° plies. The thinnest 90° plies that have been tested were for the 90° plies being half the thickness of the 0° plies [11]. Microcrack suppression would probably occur as well for carbon epoxy laminates if experiments were done for laminates with thinner 90° ply groups. The specific thickness for suppression probably differs from that for glass/epoxy laminates because of the different stiffnesses of carbon and glass.

Besides $[0_n/90_m]_s$ laminates, microcracks may initiate in the 90° plies of any laminate [11, 12]. For example, Flaggs and Kural [11] studied microcracking in $[\pm 30/90_n]_s$ and $[\pm 60/90_n]_s$ laminates in addition to $[0_2/90_n]_s$. There has also been work on $[90_n/0_m]_s$ laminates or cross-ply laminates with the 90° plies on the surface instead of in the middle [6, 13–19]. The universal observation is that the microcracking properties of $[90_n/0_m]_s$ laminates differ from those of the corresponding $[0_m/90_n]_s$ laminate. In particular, the strain to initiate microcracking is lower for laminates with surface 90° plies than for laminates with the central 90° plies. The results from $[0/90]_s$ laminates (see Fig. 1) show that the supporting plies constrain the 90° plies and can inhibit microcracking. Surface 90° plies, however, are only constrained on one side and thus microcracking initiates easier. The difference between surface and central 90° plies is another example of the problem of first-ply failure models. In laminated plate theory calculations for $[90_n/0_m]_s$ and $[0_m/90_n]_s$ laminate, the strains in the 90° plies are unaffected by the stacking sequence. Thus, first-ply failure models can not predict the different microcracking properties of these two types of similar laminates.

There have been a few attempts to account for the variations in strain to initiate microcracking by introducing statistical strength arguments [20–24]. For example, as the thickness of the 90° plies decreases, the smaller volume of ply material will have statistically fewer flaws and thus will naturally show a higher strain to failure. Statistical strength models can do a good job at fitting some experimental results [23, 24], but there are some serious drawbacks. First, like first-ply failure models, statistical strength models must resort to *in situ* statistical fitting parameters. The use of *in situ* properties limits predictive capabilities. Second, statistical models can not predict the differences between $[90_n/0_m]_s$ and $[0_m/90_n]_s$ laminates. In fact, any statistical analysis should predict microcracking in the surface (90_n) ply group to happen at a *higher* strain then in the corresponding central (90_{2n}) ply group because the surface ply group is smaller and therefore will have statistically fewer flaws.

2.13.2.2 Multiple Microcracking

The first microcrack causes very little change in the thermomechanical properties of the laminate. Continued loading, however, normally leads to additional microcracks and continued degradation in thermomechanical properties. A logical experiment to characterize the microcracking properties of laminates is to follow the microcracking process and record the number of cracks or microcrack density as a function of applied load. Such microcrack density experiments have been done on many different systems [1, 2, 4, 6, 7, 12, 14, 17, 22–44]. This section will describe the main features of multiple cracking experiments by describing the study in Ref. [42] that studied the most number of different laminates, 21 different layups, for a single material system, AS4/3501-6, carbon epoxy laminates. Other results as a function of laminate stacking sequence in the literature show the same trends as the results in Ref. [42].

Some multiple microcracking results for several different $[0_n/90_m]$ AS4/3501 carbon/epoxy laminates are given in Fig. 2. For all laminates, the characteristic microcracking curve has no microcracks until some onset stress that corresponds to the initiation of microcracking. After the initial microcrack, the microcrack density typically increases very rapidly. At high crack density, the microcracking slows down and approaches a saturation damage state. The initial rapid rise varies between different material types with some laminates having a slower increase in crack density or a more sigmoidal shape than other laminates. The rate of the initial rise has been associated with manufacturing defects or statistical inhomogeneities in the ply material [1, 41, 42]. In other words, a broadening of the rising portion of the microcrack density curve probably indicates laminates with more statistical variability than laminates with a more rapid rise

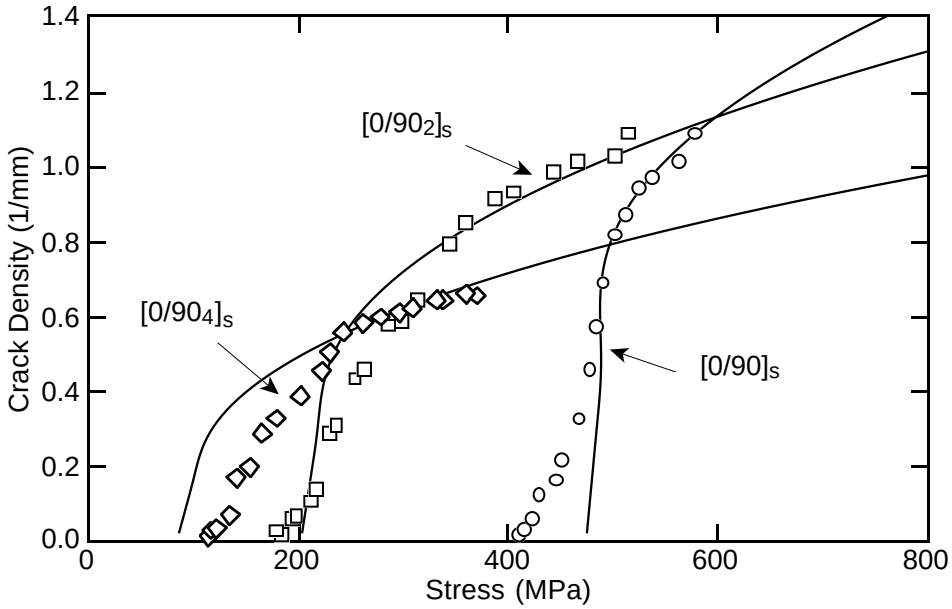

Figure 2 Microcrack density as a function of applied stress for three AS4/3501-6, $[0/90_n]_s$ laminates. The symbols are experimental results. The lines are fits to the experiments using the fracture mechanics analysis of microcracking with $G_{mc} = 250 \pm 10$ J/m^2 and assuming fixed-displacement boundary conditions.

in microcrack density. Well-made carbon/epoxy laminates, such as those used for the result in Fig. 2 typically have a rapid rise in microcrack density. Laminates with thermoplastic matrices that are harder to manufacture with uniform fiber distributions typically have a slower rise in crack density [41]. Some analysis methods to account for statistical variations in microcracking properties are discussed later in this chapter.

The three experiments in Fig. 2 are for laminates with the same thickness of 0° plies but different thicknesses of 90° plies. The onset stress decreases as the thickness of the 90°plies increases. This effect is another observation of the microcracking initiation properties discussed above where microcracks form more easily in thicker 90° ply groups or microcracking is suppressed in thin 90° ply groups. On continued loading, however, the situation reverses — thinner 90° ply groups eventually develop more microcracks than thicker 90° ply groups. In other words, the saturation crack density is inversely related to the thickness of the 90° plies. Some analogous microcracking experiments on very thin, 50–100 nm, SiO_x coatings on polymeric substrates yields final crack densities of 200 cracks/mm suggesting that an inverse relation between layer thickness and saturation crack density is general for microcracking phenomena [45, 46]. Finally, the smooth lines in Fig. 2 are fits to the experiments using a fracture mechanics analysis of microcracking that is discussed below.

As observed for microcrack initiation properties, the multiple microcracking properties of $[90_m/0_n]_s$ laminates differ from those of the corresponding $[0_n/90_m]_s$ laminates. Some typical results for four different $[90_m/0_n]_s$ AS4/3501-6 carbon/epoxy laminates are given in Fig. 3. The characteristic curves are the same as for $[0_n/90_m]_s$ laminates — after an onset of microcracking there is a rapid rise in microcrack density followed by a slowing towards microcracking saturation at high applied loads. The four experiments in Fig. 3 are for laminates with the same thickness of 90° plies but different thicknesses of the 0° plies. These results show that the microcracking properties of a laminate are not just a property of the thickness of the 90° plies; the properties also depend in the thickness and mechanical properties of the supporting plies. Comparing the results for the $[0/90]_s$ and $[90/0]_s$ laminates in Figs. 2 and 3, which are the same laminate tested in two different directions, shows that microcracks start sooner in $[90_m/0_n]_s$ laminates but that $[0_n/90_m]_s$ laminates eventually develop more microcracks at saturation [17–19].

Another important difference between $[0_n/90_m]_s$ and $[90_m/0_n]_s$ laminates is the final characteristic damage state. In $[0_n/90_m]_s$ laminates, there is only one ply group that microcracks and it develops a roughly periodic array of microcracks (see Fig. 4A). In contrast, $[90_m/0_n]_s$ laminates have two microcracking ply

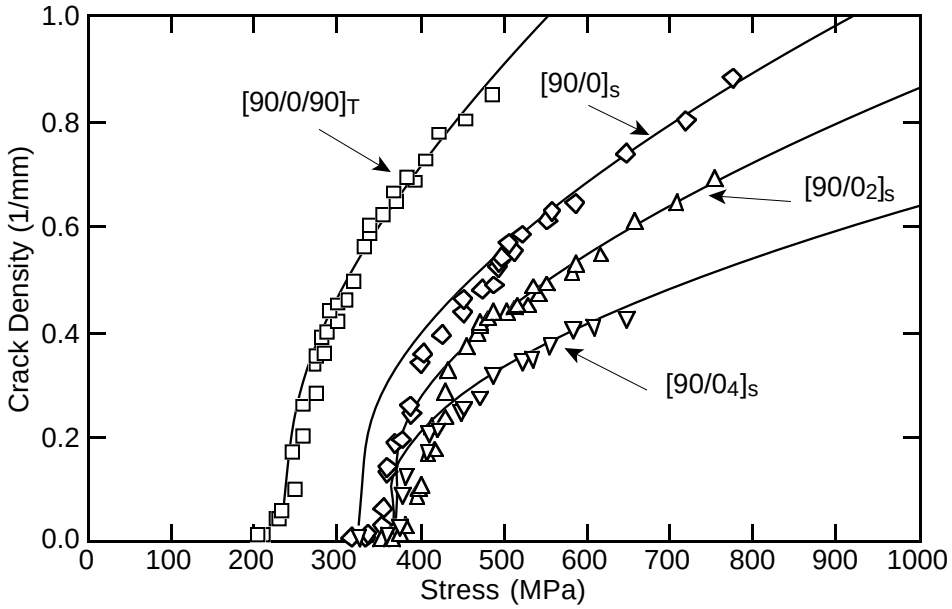

Figure 3 Microcrack density as a function of applied stress for four AS4/3501-6, $[90/0_n]_s$ laminates. The symbols are experimental results. The lines are fits to the experiments using the fracture mechanics analysis of microcracking with $G_{mc} = 230 \pm 10$ J/m^2 and assuming fixed-displacement boundary conditions.

groups. They each develop roughly periodic arrays of microcracks, but the microcracking pattern in one ply group tends to be staggered, rather than aligned, with the microcracking pattern in the other ply group [1, 17, 14] (see Fig. 4B). The development of antisymmetric or staggered microcracks can be explained by consideration of the stress state in $[90_m/0_n]_s$ laminates [17]. Any analysis that expects to explain the difference between $[0_n/90_m]_s$ and $[90_m/0_n]_s$ laminates must be able to account for the differing damage patterns. For example, the smooth lines in Fig. 3 are fits to the experiments using a fracture mechanics analysis of microcracking that is discussed below and accounts for staggered microcracks.

The initial stages of damage in laminates with 90° plies is mostly microcracking in the 90° plies. As the load increases, however, other forms of damage begin to occur. For example, the tip of the microcrack at the 0/90° ply interface provides a site for initiation of delamination between the 0° and 90° plies [1, 15, 16, 18, 25, 26, 28, 29, 31, 32, 34, 39, 47–54]. Delamination from the tips of microcracks can occur in almost any laminate but its likelihood increases as the thickness of the 90° plies increases [1, 25, 26, 28, 48, 49, 51]. If the 90° plies are thick enough, it is possible for delamination to initiate from the first microcrack. Once delaminations begin to form, they propagate on continued loading while additional microcracking slows down or stops [54]. Poisson effects during axial loading of $[0_n/90_m]_s$ laminates leads to tensile stresses perpendicular to the fibers in the 0° plies. If the applied strain gets sufficiently high, this transverse stress can lead to longitudinal splits in the 0° plies [5, 6, 34, 51]. Such longitudinal splits are more common for experiments on glass/epoxy laminates than on carbon/epoxy laminate because the glass/epoxy laminates can be loaded to higher strains before final failure [5, 6]. When $[0_n/90_m]_s$ laminate plates are subjected to biaxial loading, or to changes in thermal loading which induces a biaxial stress state, microcracks develop in all plies [55–58]. The microcracks in the 0° plies are analogous to the longitudinal splits observed in uniaxial tests.

At high crack densities, periodic microcracking is sometimes replaced by curved cracks located near existing straight microcracks [1, 34, 59]. Such curved cracks are illustrated in Fig. 4C. Some details about curved microcracks can be explained by consideration of the principal stresses in the 90° plies [34]. At low crack density, both the maximum axial stress and maximum principal stress in the 90° plies occurs midway between existing microcracks. Thus, at low crack density there is a tendency for new cracks to form midway between existing microcracks and develop into a periodic array of microcracks. At high crack density, however, interactions between microcracks causes the maximum principal stress to shift to a location

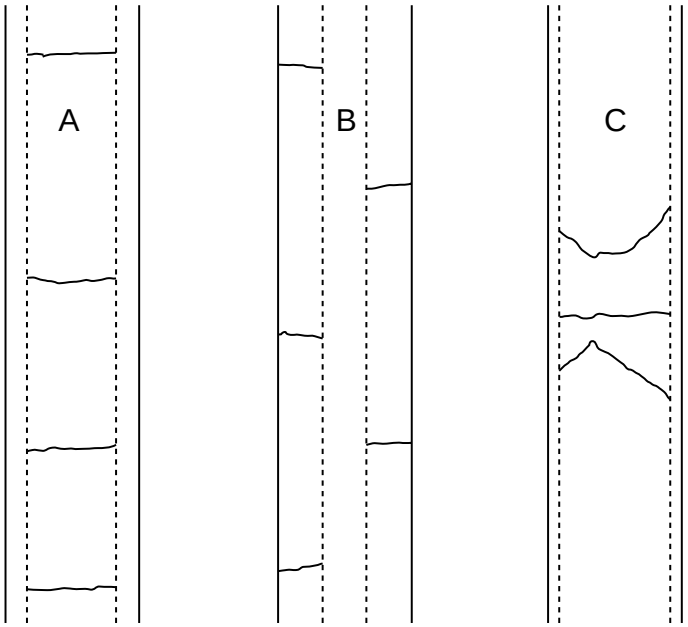

Figure 4 Sketches of actual edge views of typically damaged cross-ply laminates. A. Roughly periodic array of microcracks in a $[0/90_4]_s$ laminate. B. Antisymmetric or staggered microcracks in a $[90_4/0_2]_s$ laminate. C. Two curved or oblique microcracks near one straight microcrack in a $[0/90_8]_s$ laminate

near the 0/90 interface and close to an existing crack [34, 59]. Both the location, relative to the existing microcrack, and the shape of curved microcracks can be predicted by considering the location and trajectory of the principal stresses in the 90° plies [34, 59].

Similar principal stress effects have been noticed for microcracking in $[0/+\theta/-\theta]_s$ laminates [53]. When $\theta = 90°$, the results are similar to other microcracking experiments with straight microcracks across the 90° plies. As θ is made smaller than 90°, however, 3D stress analysis shows that the principal stress trajectories in the off-axis, θ plies is no longer straight. It has been postulated that these curved stress trajectories account for the observation of curved microcracks at low crack density in $[0/+\theta/-\theta]_s$ laminates. Another observation about microcracking in $[0/+\theta/-\theta]_s$ laminates is that when $\theta = 90°$, microcracks always propagate rapidly across the entire cross section of the 90° plies. As θ is reduced, however, the microcracks initiate on the edge but only propagate part way into the laminate. Such curved and angled edge cracks typically cause edge delaminations soon after their initial formation [53].

2.13.2.3 Loading and Environmental Effects

Most microcracking experiments have been done using uniaxial tension, but microcracks will also form under other loading conditions. For example, microcracks will form in the 90° plies on the tension side of a laminate subjected to bending [60]. The results in bending are qualitatively similar to results in tension, but analyses of bending experiments need to account for the different stress state in laminates under bending than in laminates under tension [61–64].

Biaxial loading of $[0_n/90_m]_s$ is similar to two uniaxial tests — one on a $[0_n/90_m]_s$ laminate and one on $[90_n/0_m]_s$. Thus microcracks may appear in both the central plies and the surface plies. The relative amount of cracking between the ply groups will depend on the ratio n to m. One natural method for inducing biaxial stresses is to subject a laminate to a change in temperature. The differential shrinkage between the 0 and 90° plies will induce biaxial loading as ΔT is increased [43, 55, 56, 65–69]. Such experiments demonstrate that residual stresses play an important role in the microcracking process of laminates. Besides residual stresses due the thermal shrinkage, the presence of moisture can induce residual stresses that influence microcracking [69–71]. In some polyimide matrix composites, hygrothermal aging causes degradation of the

matrix [70, 71]. Eventually the toughness of the matrix drops sufficiently low that spontaneous microcracks form due to residual stresses alone [70, 71].

Most microcracking experiments have been conducted on laminates under uniform stress states such that the stress state in the 90° plies is uniform prior to microcracking. These stress states typically cause rapid crack growth across the entire cross section of the 90° plies. If laminates with 90° plies have stress concentrations such as holes, it is possible to observe microcracks forming at the edge of the hole and propagating into the laminate [72, 73]. For such a non-uniform stress state, the microcrack driving force decreases as the crack moves away from the hole. Therefore, the microcracks arrest and produce a damage zone around the hole. In one case-study on the durability of an I-beam with circular cut-outs, the microcracking process around the holes was a major factor in the lifetime of the beam [73].

2.13.2.4 Fatigue Observations

Fatigue loading of laminates with 90° plies also leads to microcracking in the 90°plies [1, 12, 13, 14, 32, 35, 38, 58, 74–84]. The typical experiments are to count the number of cracks as a function of cycle number. The number of cracks increases with cycling. Eventually fatigue loading also leads to the other damage mechanisms observed in static testing such as curved microcracks, delaminations from the tips of microcracks, and longitudinal splits in the supporting plies.

Microcrack propagation is slightly different during fatigue as compared to microcrack propagation during static loading. In static loading, microcrack propagation is governed by the thickness of the 90° plies. When the 90° plies are thick, the microcrack propagation is instantaneous; when the 90° plies are thin, the microcrack propagation is controlled or perhaps even suppressed. During fatigue loading, microcrack propagation depends similarly on thickness of the 90° plies but also depends on the amplitude of the fatigue stress. During high-cycle fatigue, or fatigue at low cyclic stress, new microcracks initiate at the specimen edge and propagate slowly across the specimen width. During low-cycle fatigue, or fatigue at high cyclic stress, microcracks that initiate at low microcrack density span the 90° ply width instantaneously as in static loading, but microcracks that initiate at high microcrack density, initiate at the specimen edges and propagate slowly across the specimen width. Observations of slowly propagating microcracks suggests that the crack growth rate per cycle is constant for each individual microcrack but depends on the distance of that microcrack to the neighboring, existing microcracks [32, 35, 38, 79]. Such observations suggest that the stress intensity factor or energy release rate for the propagating microcrack is independent of the length of the microcrack and only a function of the space between existing microcracks where the microcrack is growing [38, 77, 79, 82].

Microcracks also form as a function of cycle number during thermal cycling of laminates [1, 16, 55, 56, 57, 58, 66–69, 85, 86]. Like mechanical fatigue, the typical experiment is to count the number of microcracks as a function of cycle number. Although the driving forces for fatigue damage in thermal cycling are similar to those during uniaxial mechanical fatigue experiments, there are some important differences. First, thermal cycling induces biaxial loading while mechanical cycling is predominantly axial loading. Second, thermal cycling subjects a laminate to a range in temperature. Temperature effects such as physical aging or thermal degradation at high temperature, embrittlement at low temperature, and other temperature dependent mechanical properties, normally causes the thermal cycling results to differ from the corresponding mechanical fatigue results [16].

2.13.3 METHODS OF ANALYSIS

Microcracking in off-axis plies is a common damage mechanism for composite laminates. It is thus important to develop analysis methods for predicting microcracks and for designing with laminates that might have microcracks. These analysis methods have two separate goals. The first goal is to consider a laminate with a given amount of microcracking and predict the *effective* thermomechanical properties of that laminate. The second goal, the more difficult goal, is to predict the conditions for which the microcracks form in the first place. This section will begin with the second goal or with the problem of developing failure models for predicting the formation and evolution of microcracking. Some failure models can be expressed in terms of *effective* thermomechanical properties of the laminate. Thus, once such failure models are developed, much

of the *effective* properties model will have already been solved as a prerequisite. This section will end with some additional comments about *effective* properties of microcracked laminates.

This chapter, and specifically the following section on methods of analysis, focuses on microcracking of 90° plies in which the laminate is predominantly loaded with tensile loads perpendicular to the fibers in those plies. There are several reasons for this approach. In such laminates, the microcracks that form in the 90° plies typically span the entire cross-section of the 90° plies. Thus the potentially three-dimensional problem can be reduced to two dimensions by looking at the edge of the laminate. Due to this simplification, the theory for such microcracking is more advanced then theories for more general forms of microcracking damage. In fact, many results for energy calculations and effective thermoelastic properties can be reduced to a single underlying problem of finding the effect of fully-developed microcracks on the effective axial modulus of the laminate. Although the analysis methods deal only with 90° ply cracking, the general principles are adaptable to more general microcracking problems in more general laminates. This adaptation, however, requires accounting for microcracks in off-axis plies, for microcracks that do not extend across the full cross-section of the cracked plies, for possibly curved microcrack shapes, and for interactions between cracks and delaminations in neighboring plies. In general, accounting for such effects requires the solution of three-dimensional stress analysis problems.

2.13.3.1 Failure Models and Finite Fracture Mechanics

Early work on microcracking assumed that microcracks form when the stress in the 90° plies reaches the transverse strength of the ply material. [2, 4, 20-22, 24-27]. Similarly, first-ply failure models in laminated plate theory models assume the ply transverse strength or some multi-axial stress state criterion determines microcrack formation [9]. As discussed in Section 2.12.2.1, the microcracking properties of laminates can not be explained in terms of strength because the stresses in the 90° plies at the onset of microcracking are not constant between different laminates [11]. In other words, there is no material property, such as a *transverse strength*, that can predict failure of plies within laminates. All strength models, including statistical strength models [20–24], must resort to using *in situ* strength properties or strength properties that are different, and therefore must be measured, for each stacking sequence.

More recent work has proposed energy methods or a fracture mechanics approach to predicting microcracking [4, 6, 15-18, 87-96]. Most energy models use a discrete model or a finite fracture mechanics model [95–97] in which the next microcrack is predicted to form when the total energy released by the formation of that microcrack reaches the critical energy release rate for microcracking, G_{mc}, or the microcracking fracture toughness. When a finite fracture mechanics model of microcracking is done correctly, it can predict results for a wide variety of laminates from a single value of G_{mc}. For example, the results in Figs. 2 and 3 in the **Multiple Microcracking** are results for seven different AS4/3501-6 laminates. All results can be fit with a G_{mc} in the range of 220–260 J/m^2. In other words, $G_{mc} = 240 \pm 20$ J/m^2 is a material property for AS4/3501-6 laminates that characterizes the sensitivity of that material to microcracking.

Although the energy model for microcracking is based in fracture mechanics and energy release rate methods, it is an unconventional application of fracture mechanics. Conventional fracture mechanics deals with crack propagation [100]. Most microcracking damage, however, occurs by fracture events in which full microcracks appear instantaneously on the experimental time scale. Besides microcracking, various other forms of composite damage such as fiber breaks [98] and interfacial debonds [99], also form as fracture events. The question arises — how can one model fracture events? One approach is to abandon fracture mechanics because there is no observable crack growth and no crack-tip singularity to analyze. For microcracking, however, when fracture mechanics is abandoned in favor of strength models, the results are unsatisfying. An alternative approach is to try to generalize fracture mechanics to deal with fracture events as well as crack propagation. Hashin [95] has recently termed such an extension of fracture mechanics as *Finite Fracture Mechanics* because it extends fracture mechanics to handle failure by events that involve a *finite* amount of new fracture area. In contrast, conventional fracture mechanics always deals with an *infinitesimal* amount of crack growth.

Developing a finite fracture mechanics model for microcracking requires two steps. First, the model requires stress analysis to calculate the total energy released by the formation of the next complete microcrack, which will be denoted here as G_m. Once this energy release rate is known, finite fracture mechanics can be used to predict the conditions required to form microcracks or to predict the experimental results for crack

density as a function of applied loads. To make these predictions, the theoretical result for G_m is equated to G_{mc}, the microcracking fracture toughness, and the resulting equation is solved for applied load. The second step to analyzing microcracking is to verify that the concept of finite fracture mechanics is a valid failure model for predicting microcracking events. In other words, before the finite fracture mechanics approach can be used, it must be verified to be correct by comparison of predictions to experimental results.

There is good reason to believe that finite fracture mechanics is a viable approach for analysis of microcracking. From the first-law of thermodynamics and energy balance arguments, it has been proposed that finite fracture mechanics should work best for a series of similar fracture events [97]. The key concept is that fracture events may release kinetic energy. Kinetic energy is apparent through the observation of acoustic emission events but it is very difficult to calculate and include kinetic energy effects in the fracture mechanics energy balance. If the total kinetic energy associated with each crack is roughly constant, however, it can be treated as part of an *effective* event toughness. In other words, the stress analysis ignores kinetic energy effects in G_m, but includes it in G_{mc}. Because microcracking is a series of similar fracture events, it is logical to assume the kinetic energy associated with each crack will be roughly constant. The verification step in finite fracture mechanics models can test this hypothesis for microcracking or for any damage mode. If a good stress analysis for energy release rate can predict experiments using a constant G_{mc}, then it can experimentally be claimed that kinetic energy is roughly constant (or negligible, in which case it is irrelevant) and that finite fracture mechanics is a valuable analysis method. If the predictions do not agree with experiments, then either the kinetic energy effects are not constant (and not negligible) or the stress analysis used to find energy release rate is not accurate. The next two sections discuss energy release rate calculations for microcracking and comparisons of model predictions to experimental results. When energy release rate is calculated with sufficient accuracy, finite fracture mechanics is an accurate tool for predicting microcracking properties of laminates.

2.13.3.2 Energy Release Rate

The key problem to analyze for a finite fracture mechanics model of microcracking in the 90° plies of $[(S)/90]_s$ laminates, where (S) is any set of supporting plies, is illustrated in Fig. 5. Figure 5A shows a unit cell of damage as the zone between two existing microcracks; figure 5B shows the same unit cell but with a new microcrack formed at the location of highest stress which is midway between the previous existing microcracks. The key problem is to calculate the total energy released per unit crack area due to the formation of the new microcrack in the unit cell of damage. That energy release rate is denoted here as G_m. Note that the loading conditions in Fig. 5 are expressed as either ε_0 or σ_0 to express experiments carried out using displacement control (ε_0) or load control (σ_0). In conventional fracture mechanics with infinitesimal amounts of crack growth, the energy release rate is independent of the loading method. In finite fracture mechanics with a finite amount of new crack area, however, G_m depends on loading method and thus the analysis must use loading conditions that match the experimental loading conditions.

Recent work on fracture analysis of composites has derived exact results that are helpful in calculating energy release rates for composite fracture events [96]. One effective tool is to partition the stresses into the initial stresses existing before the fracture event and the perturbation stresses, or the change in stresses caused by the fracture event. Using the stress partitioning methods of Ref. [96], the microcracking energy release rate under constant strain (displacement control) can be written exactly as

$$G_m = \frac{1}{2}\sigma^0_{xx,1}\Big[2\left\langle\delta(\rho/2)\right\rangle - \left\langle\delta(\rho)\right\rangle\Big] \tag{1}$$

where $\sigma^0_{xx,1}$ is the initial stress in the 90° plies at the location of the microcrack before any microcracks form and $\langle\delta(\rho)\rangle$ is the average crack opening displacement for a microcrack in a unit cell of damage of aspect ratio $\rho = a/t_1$ (see Fig. 5). From the potential energy results in Ref. [96], it is possible to express the effective axial modulus for a unit cell of aspect ratio ρ, $E_A(\rho)$, in terms of the average crack opening displacement in that cell as

$$E_A(\rho) = E_{A0} - \frac{E^2_{xx,1}\left\langle\delta(\rho)\right\rangle}{\sigma^0_{xx,1}\rho B} \tag{2}$$

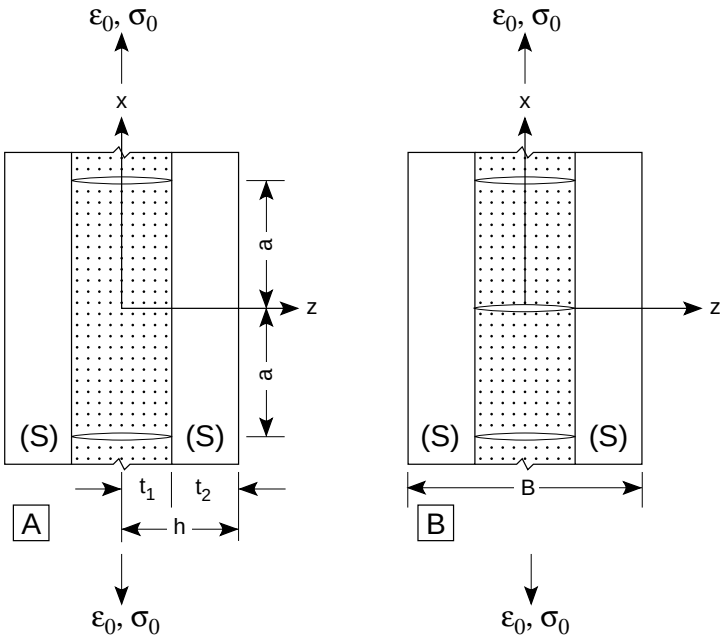

Figure 5 A unit cell of damage for microcracking in $[(S)/90_n]_s$ laminates. A. Two existing microcracks spaced by a distance $2a$. The aspect ratio of the microcracking interval is $\rho = a/t_1$. B. The same laminate after formation of a new microcrack midway between the existing microcracks.

where E_{A0} is the effective axial modulus in the absence of microcracks, $E_{xx,1}$ is the x-direction modulus of the 90° plies, $B = 2h$ is the thickness of the laminate.By substituting Equation (2) into Equation (1) the energy release rate for microcracking under displacement control can be written as

$$G_m = -\frac{1}{2}\rho B \left(\frac{\sigma^0_{xx,1}}{E_{xx,1}}\right)^2 \left[E_A(\rho/2) - E_A(\rho)\right] \qquad \text{(displacement control)} \tag{3}$$

A similar type of analysis but for load control conditions was derived in Ref. [101]; the result is

$$G_m = \frac{1}{2}\rho B E^2_{A0} \left(\frac{\sigma^0_{xx,1}}{E_{xx,1}}\right)^2 \left[\frac{1}{E_A(\rho/2)} - \frac{1}{E_A(\rho)}\right] \qquad \text{(load control)} \tag{4}$$

Clearly effective modulus, $E_A(\rho)$, is a material property that does not depend on loading conditions. The energy release rate, G_m, is a function of $E_A(\rho)$, but that function depends on loading conditions and thus G_m depends on loading conditions.

By using Equations (1), (3), and (4), the energy release for displacement control and for load control can each be expressed exactly either in terms of average crack opening displacement or in terms of the effective axial modulus of a laminate with periodic microcracks. Thus, once crack opening displacement or effective properties of a microcracked laminate are known, the energy release rate for microcracking can be calculated. It is important to note that G_m for displacement control is not equal to G_m for load control. The difference is a consequence of microcracking involving a finite amount of fracture growth in contrast to conventional fracture mechanics which analyzes an infinitesimal amount of crack growth. The boundary condition effect is illustrated in Fig. 6 which plots loading and unloading load-displacement curves for a finite amount of fracture growth. The total energy released is the area between the loading and unloading curves [102].

For fixed-load boundary conditions, the total energy released is equal to the area of the ABC triangle; for fixed-displacement boundary conditions, the total energy released is lower and equal to the shaded area of the ABD triangle. Clearly, the energy released for fixed-displacement conditions is different and less than

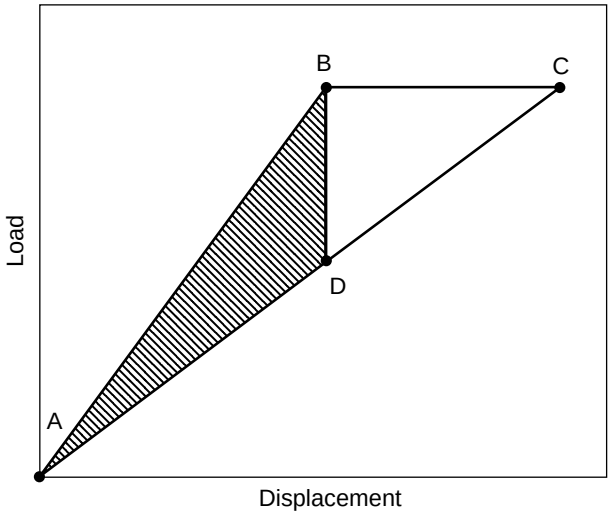

Figure 6 Load-displacement curve for a finite increase in crack area. The area of the ABC triangle is the total energy released by crack growth under load control. The shaded area of the ABD triangle is the total energy released by crack growth under displacement control.

the energy released for fixed-load conditions. In the limit of infinitesimal fracture area, the areas become equal to each other or the energy release rate for conventional fracture mechanics is independent of loading conditions. When analyzing real experiments with finite fracture area, however, it is important to use the correct result for the specific experimental conditions. Similarly, the displacement and load control results for microcracking are the same in the limit of zero microcrack density. When analyzing any microcracking experiment, except initiation of the first microcrack, however, it is important to use the correct energy release rate equation. Most static microcracking tests are done under displacement control while most fatigue tests are done under load control. Thus G_m in Equation (3) should be used for analysis of static tests while G_m in Equation (4) should be used for analysis of fatigue tests. Some consequences of using the wrong G_m will be discussed below.

The energy release rate results in Equations (3) and (4) are exact results for a two-dimensional plane stress analysis of the cracked laminate assuming an exact result for $E_A(\rho)$ is known. These results can be converted to an exact two-dimensional plane strain analysis by replacing ply properties with reduced ply properties. These two-dimensional results, however, ignore possible three dimensional effects caused by differential Poisson contraction between the 90° plies and the supporting plies in the z direction. It is possible to extend the above two-dimensional methods to account for three-dimensional effects. The resulting energy release rates then depends on effective axial modulus ($E_A(\rho)$), effective transverse modulus ($E_T(\rho)$), and effective in-plane Poisson's ratio ($\nu_{xz}(\rho)$) of the microcracked laminate instead of just on the effective axial modulus [107–109]. The additional terms involving $E_T(\rho)$ and $\nu_{xz}(\rho)$ correct for differential Poisson's effects and are generally small. This chapter will use the simpler two-dimensional results to interpret experimental results.

The finite fracture mechanics analysis for laminates with 90° plies on the surface ($[90_n/(S)]_s$ laminates), needs to account for the development of staggered microcracks in the two 90° ply groups. The key problem to analyze for microcracking in $[90/(S)]_s$ laminates is illustrated in Fig. 7. Figure 7A shows a unit cell of damage with staggered microcracks. It is not possible to add a single new microcrack to the unit cell while still representing the damage laminate with unit cells of damage. Instead, microcracking of $[90/(S)]_s$ laminates can be analyzed by considering the new state in Fig. 7B where enough new microcracks are formed to generate three unit cells of damage from the initial single unit cell of damage. By the methods used to analyze $[(S)/90_n]_s$ laminates, the energy release rate for the discrete fracture process illustrated in Fig. 7 using a two-dimensional analysis under displacement control can be written exactly as

$$G_m = -\frac{1}{4}\rho B\left(\frac{\sigma^0_{xx,1}}{E_{xx,1}}\right)^2\Big[E_A(\rho/3) - E_A(\rho)\Big] \qquad \text{(displacement control)} \tag{5}$$

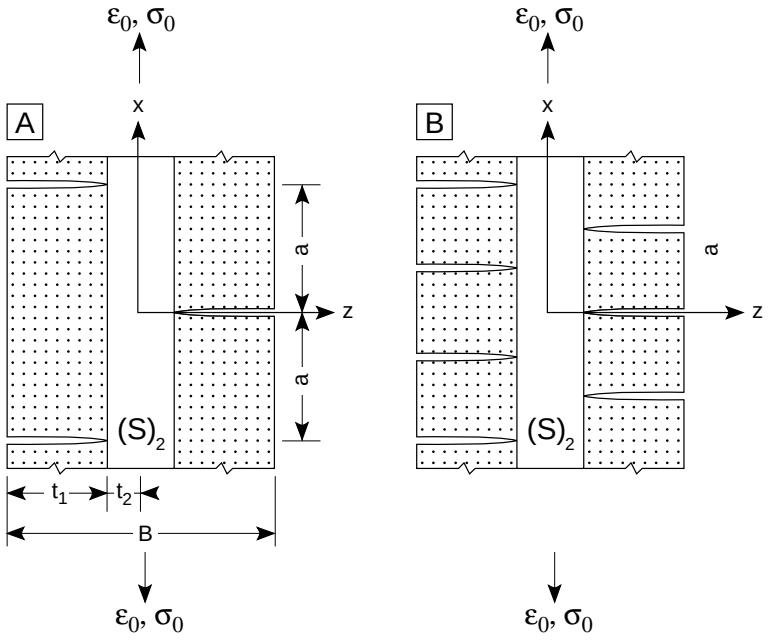

Figure 7 A unit cell of damage for microcracking in $[90_n/(S)]_s$ laminates. A. Two staggered microcracks spaced by a distance $2a$ on each side of the laminate. The aspect ratio of the microcracking unit cell is $\rho = a/t_1$. B. The same laminate after formation of a four new microcracks convert the single unit cell of damage into three unit cells of damage.

For load-control conditions, the result is

$$G_m = \frac{1}{4}\rho B E_{A0}^2 \left(\frac{\sigma^0_{xx,1}}{E_{xx,1}}\right)^2 \left[\frac{1}{E_A(\rho/3)} - \frac{1}{E_A(\rho)}\right] \qquad \text{(load control)} \tag{6}$$

Thus, the energy release for formation of microcracks in $[90_n/(S)]_s$ laminates is different than in $[(S)/90_n]_s$ laminates. The form of the G_m equations are different and the analysis method for finding $E_A(\rho)$ should account for the presence of staggered microcracks in $[90_n/(S)]_s$ laminates. In other words, $E_A(\rho)$ for $[90_n/(S)]_s$ laminates will be different than $E_A(\rho)$ for $[(S)/90_n]_s$ laminates. The experimental observation is that the microcracking properties of $[90_n/(S)]_s$ and $[(S)/90_n]_s$ laminates are different; finite fracture mechanics can potentially explain those differences. The G_m results for $[90_n/(S)]_s$ laminates could alternatively be expressed in terms of average crack opening displacement instead of in terms of effective axial modulus. Finally, these two-dimensional results could be extended to include three dimensional effects. Like the analysis of $[(S)/90_n]_s$, however, the three-dimensional Poisson effects on G_m are small.

Experimental observations show that the microcracking process is influenced by the presence of residual stresses. All residual stress effects are included in the above analyses through the $\sigma^0_{xx,1}$ term or the initial stress in the 90° plies. This initial stress is the *total* initial stress or the sum of mechanically applied stresses and residual stresses in the 90° plies of the undamaged laminate. All G_m expressions can be written in terms of the effective axial modulus, $E_A(\rho)$. For linear thermoelastic materials, $E_A(\rho)$ is independent of the level of residual stresses and thus can be found by stress analysis methods that ignore residual stresses. Once the results are substituted into the G_m expressions along with $\sigma^0_{xx,1}$, however, the resulting G_m gives the total energy release rate or the energy release rate due to both mechanical and residual stresses.

There are other generalized analyses of microcracking that can be shown to be equivalent to the above discussion but are in a different form. These other results required longer derivations while the above analysis was a straightforward application of the results in Ref. [96]. For example, McCartney [107, 108] considered

triaxial loading and was able to express many results in terms of a "damage" parameter $\Phi(\omega)$ defined by

$$\Phi(\omega) = \frac{1}{E_A(\omega)} - \frac{1}{E_{A0}} \tag{7}$$

where ω expresses the state of damage. McCartney's analysis considered load-control experiments only; clearly the load-control G_m result in Equation (4) could likewise be expressed in terms of $\Phi(\omega)$. McCartney's analysis does not include analysis of cracking in surface plies ($[90_n/(S)]_s$ laminates), but it does extend the above results for triaxial stress states and for Poisson effects. Varna [110–115] choose to express modulus and energy release rate in terms of average crack opening displacement. Because of relations like Equations (1) and (2) most important results for analysis of microcracking can be reduced to the problem of finding either the average crack opening displacement or the effective axial modulus each as a function of microcracking spacing. Results in terms of either average crack opening displacement or effective modulus are exact and equivalent.

2.13.3.3 Master Plot Analysis

The energy release rate equations for G_m in the previous section and the principles of finite fracture mechanics can be used to predict the formation of microcracks for a wide variety of laminates with 90° plies and for experiments under differing loading conditions. These predictions need to be verified by comparison to experiments. In other words, finite fracture mechanics is an unconventional fracture analysis technique for composites. Before it can be used for predictions of any class of fracture events, it must be verified that the predictions agree with a wide range of experimental results. This section describes a master plot analysis method that can critically test both the applicability of finite fracture mechanics to analysis of microcracking and the accuracy of various stress analysis methods to determine G_m. The accuracy of the G_m calculations depends on the accuracy of the stress analysis methods used to calculate $E_A(\rho)$ (or $\langle\delta(\rho)\rangle$).

For both $[(S)/90_n]_s$ and $[90_n/(S)]_s$ laminates and for both displacement-control and load-control experiments, the energy release for the formation of the next microcrack can be written generically as

$$G_m = \left(\sigma^0_{xx,1}\right)^2 G_{unit}(\rho) \tag{8}$$

where $G_{unit}(\rho)$ is the energy release rate for formation of new microcracks in a unit cell of damage of aspect ratio ρ when there is unit stress in the 90° plies in the absence of microcracking. $G_{unit}(\rho)$ will change depending on laminate type and loading conditions, but the generic form of G_m will remain the same. For linear thermoelastic materials, the initial stress in the 90° plies can be written as

$$\sigma^0_{xx,1} = k_{m,1}\sigma_0 + k_{th,1}\Delta T \tag{9}$$

where σ_0 is the total applied axial stress and $\Delta T = T_s - T_0$ is the difference between the specimen temperature, T_s, and the stress-free temperature, T_0, and $k_{m,1}$ and $k_{th,1}$ are mechanical and thermal stiffnesses for the 90° plies. These stiffnesses will depend on laminate structure and ply properties and they can easily be calculated from laminated plate theory [1]. To predict microcracking using finite fracture mechanics, we equate G_m to G_{mc}, or the microcracking fracture toughness, and solve the resulting equation for applied stress; the result is:

$$\sigma_0 = \frac{1}{k_{m,1}}\sqrt{\frac{G_m}{G_{unit}(\rho)}} - \frac{k_{th,1}}{k_{m,1}}\Delta T \tag{10}$$

For any laminate geometry and loading conditions, Equation (10) gives the stress as a function of crack density, $D = 1/(2t_1\rho)$. Inverting this result gives a prediction for crack density as a function of applied load that can be compared to experiments. McCartney [107, 108] derived a result that is equivalent to Equation (10) for axial loading, but additionally extends it for microcracking during triaxial loading.

Some typical results for comparison of Equation (10) to experimental results are given in Figs. 2 and 3. The $G_{unit}(\rho)$ required for the predictions used $E_A(\rho)$ calculated using two-dimensional variational mechanics [1, 42, 95, 103, 104]. Previous finite fracture mechanics models for microcracking were for load-control boundary conditions [1, 42]. The new predictions in Figs. 2 and 3 calculated $G_{unit}(\rho)$ for the experimental

loading conditions which were displacement control [42]. The comparison between experiments and theory shows that finite fracture mechanics does a good job of simultaneously predicting the microcracking properties for all laminates. All experimental results can be fit with a single value of $G_{mc} = 230 \pm 20$ J/m^2. Thus G_{mc} is a useful material property characterizing a particular composite material's resistance to microcracking.

There are two common discrepancies between experiments and finite fracture mechanics predictions. First, the experimental crack density often rises slower than the predicted crack density. See, for example, the experiments and predictions for $[0/90]_s$ laminates in Fig. 2. These low-crack density deviations have been attributed to flaws in the laminate or to statistical inhomogeneities in the laminate structure [1, 42]. By either mechanism, the 90° plies can be treated as having regions of lower toughness and regions of higher toughness. The lower toughness regions can be caused by flaws or by structural imperfections such as unfavorable fiber distributions. The first few microcracks form at regions of low toughness and thus deviate from the theory which assumes a single-value for G_{mc}. At higher crack density, the weak regions get used up and later predictions agree better with experimental results. Some statistical methods for dealing with variations in toughness are discussed below.

The second common deviation is that experimental results often yield higher crack density at high stress than predicted by Equation (10). This type of deviation can be explained by distributions in microcrack spacing. When the microcrack spacings are not periodic, the new microcracks will tend to form in regions with wider crack spacing because such cracks release more energy than cracks in regions with shorter crack spacings. There are two effects of this tendency for microcracks to form in regions with crack density lower than the average crack density. First, it naturally drives the microcracking process to give a roughly periodic array of microcracks. Second, it causes laminates to develop more microcracks than predicted by theory. This crack distribution effect can be corrected experimentally or can be corrected by the addition of a simple parameter that scales the *true* crack density to a slightly lower *effective* crack density [42]. There are no deviations at high crack density in Figs. 2 and 3 because these fits have all been adjusted for crack distribution effects using the methods given in Ref. [42].

Equation (10) can be recast in the following form:

$$-\frac{k_{m,1}}{k_{th,1}}\sigma_0 = -\frac{1}{k_{th,1}}\sqrt{\frac{G_{mc}}{G_{unit}(\rho)}} + \Delta T \tag{11}$$

This finite fracture mechanics prediction suggests defining a *reduced* stress, σ_R, and *reduced* crack density, D_R, as

$$\sigma_R = -\frac{k_{m,1}}{k_{th,1}}\sigma_0 \tag{12}$$

$$D_R = -\frac{1}{k_{th,1}}\sqrt{\frac{1}{G_{unit}(\rho)}} \tag{13}$$

Using laminated plate theory to find $k_{m,1}$ and $k_{th,1}$ and a stress analysis theory to find $G_{unit}(\rho)$, any set of experimental results for microcracking density as a function of applied stress can be turned into experimental results for σ_R as a function of D_R. By Equation (11), σ_R and D_R are related by

$$\sigma_R = D_R\sqrt{G_{mc}} + \Delta T \tag{14}$$

In other words, a plot of σ_R as a function of D_R is predicted to be linear. The slope of the plot will give the toughness, G_{mc}, while the intercept will give the thermal term causing the residual thermal stresses, ΔT. Furthermore, because G_{mc} and ΔT are material properties and not functions of laminate stacking sequences, experimental results from a single material, but on a wide variety of laminates including $[(S)/90_n]_s$ and $[90_n/(S)]_s$ laminates, should all fall on the same straight line or *master plot* for that material.

Master plots from microcracking experiments provide a critical test of the finite fracture mechanics analysis of microcracking. It is important to recognize that a single master plot is testing two aspects of the microcracking model. First, it is testing the applicability of finite fracture mechanics for predicting microcracking. For master plots to be linear, it is necessary that all microcracks form at nearly the same

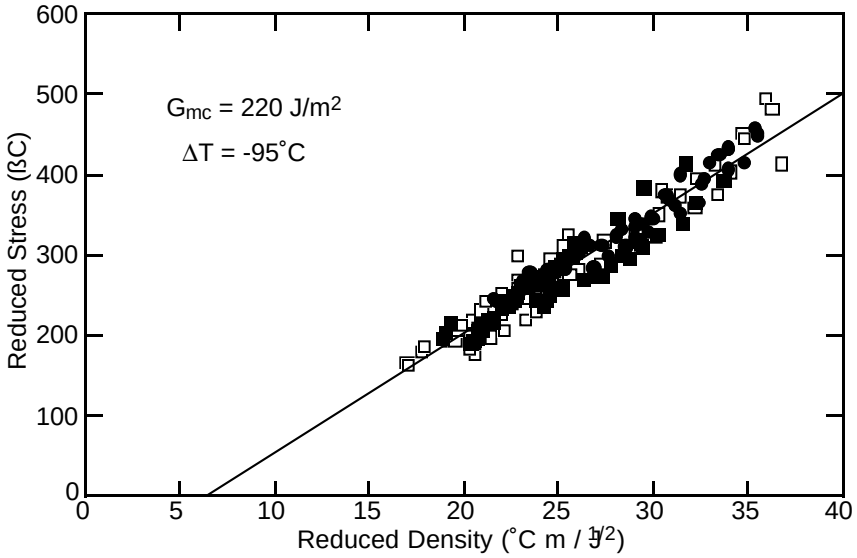

Figure 8 Master plot analysis for 14 $[0_n/90_m]_s$ (open symbols) and $[90_m/0_n]_s$ (filled symbols) AS4/3501-6 carbon/epoxy laminates. $G_{unit}(\rho)$ was calculated from a complementary energy analysis with constant displacement boundary conditions. The straight line is a linear fit to the experimental results. The slope and intercept of the fit give $G_{mc} = 220$ J/m^2 and $\Delta T = -95$°C.

value of the critical energy release rate G_{mc}. If G_{mc} is not a material property, the master plots will not be linear. Second, master plots test the accuracy of the stress analysis used to find $G_{unit}(\rho)$. In other words, even if finite fracture mechanics of microcracking is rigorously correct, master plots will not be linear if the stress analysis used to find $G_{unit}(\rho)$ is inaccurate.

Figure 8 gives a master plot for 14 different laminates of AS4/3501-6 carbon/epoxy laminates. This master plot analysis was constructed using a $G_{unit}(\rho)$ in which $E_A(\rho)$ was calculated using complementary energy methods and variational mechanics [1, 42, 95, 103, 104]. Previous master plot calculations assumed constant load boundary conditions, but these experiments were under displacement control [42]. Here, $G_{unit}(\rho)$ was adjusted to account for displacement-control experiments [96, 97]. This master plot is very linear within a relatively narrow experimental scatter band. The results for all laminates fall on the same line. Furthermore, the two-dimensional variational mechanics methods can distinguish between $[0_m/90_n]_s$ and $[90_n/0_m]_s$ laminates [17, 42]; when the disparate damage modes are correctly evaluated (periodic cracks *vs.* staggered cracks), the results for both laminate types reduce to the same master plot. From the slope and intercept of the master plot, the microcracking toughness is found to be $G_{mc} = 220$ J/m^2 and the residual stress term is found to be $\Delta T = -95$°C. Both of these results are physically reasonable which further supports the validity of the finite fracture mechanics model of microcracking. Note that master plots lets one determine toughness without any prior knowledge of the level of residual stresses in the laminate. The level of residual stresses are experimentally determined during analysis of the microcracking experiments from the intercept of the master plot.

It was mentioned above that finite fracture mechanics models need to correctly handle the boundary conditions because the amount of energy released in a fracture event depends on loading method. Most previous microcracking models incorrectly used load-control analyses to interpret static tests done under displacement control [4, 6, 15-18, 87-95]. Figure 9 shows a new master plot identical to Fig. 8 except that $G_{unit}(\rho)$ was evaluated by a two-dimensional complementary energy analysis that assumes load control. Although the load-control master plot is close to linear, there is noticeably more scatter here than in the displacement-control master plot. This boundary condition effect further supports the validity of the finite fracture mechanics model of microcracking. When the analysis is correctly refined to handle the experimental loading conditions, the master plot improves. The slope and intercept of the load-control plot give $G_{mc} = 330$ J/m^2 and $\Delta T = -143$°C. The differences in scatter between the displacement-control and the load-control analyses are not large, but the differences in evaluated toughness and residual stresses are significant.

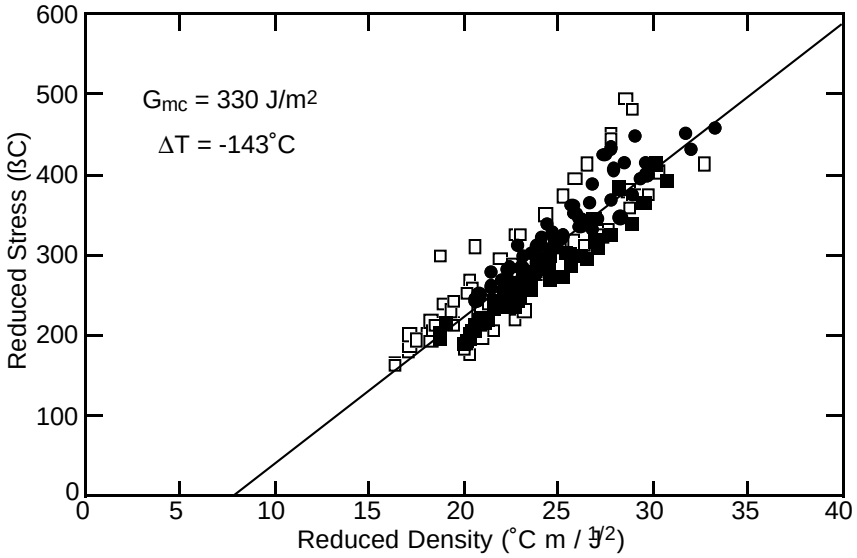

Figure 9 Master plot analysis for 14 $[0_n/90_m]_s$ (open symbols) and $[90_m/0_n]_s$ (filled symbols) AS4/3501-6 carbon/epoxy laminates. $G_{unit}(\rho)$ was calculated from a complementary energy analysis with constant load boundary conditions. The straight line is a linear fit to the experimental results. The slope and intercept of the fit give $G_{mc} = 330$ J/m^2 and $\Delta T = -143°$C.

This observation demonstrates that use of the wrong expression fo G_m can lead to errors of 30% to 50% in the evaluated microcracking toughness. The G_{mc} determined from the load-control plot is physically the wrong result. It is not the amount of energy required to form microcracks in this material.

By using Equations (3) and (5), any analysis for $E_A(\rho)$ in cross-ply laminates can be used to calculate $G_{unit}(\rho)$ and therefore used to generate master plots for microcracking. Many early microcracking models found $E_A(\rho)$ using shear lag methods (see citations in Ref. [1]). The most accurate shear-lag analysis of a microcracking laminates was recently derived by McCartney [105]. This shear-lag analysis does a good job of predicting modulus loss experiments. Figure 10 gives the master plot analysis that results when $G_{unit}(\rho)$ is found using a shear lag analysis. Although the global fitting results which lead to $G_{mc} = 225$ J/m^2 and $\Delta T = -114°$C are reasonable, the shear-lag master plot has some problems. First, the results for individual laminates do not reduce to the same master plot, but are highly scattered around the average master plot. Thus, despite the fact that shear-lag analysis does a good job of predicting $E_A(\rho)$, it does a poor job of calculating $G_{unit}(\rho)$ which is required for getting a good master plot. This apparent contradiction arises because predicting modulus reduction only involves finding $E_A(\rho)$ while finding $G_{unit}(\rho)$ requires finding differences like $E_A(\rho/2) - E_A(\rho)$. In others words, in order for $G_{unit}(\rho)$ to be accurate, the analysis to find $E_A(\rho)$ must be sufficiently accurate that its first difference (or first derivative) is also accurate. In approximate stress analyses, it is much easier to find accurate bulk properties, like modulus, then it is find accurate first derivatives as well. Thus, although shear-lag analysis is sufficiently accurate for $E_A(\rho)$, it may not be accurate enough for the derivative of $E_(\rho)$. In contrast, the two-dimensional, variational mechanics methods are sufficiently accurate for both $E_A(\rho)$ and its derivative that they can be used to find both modulus reduction and energy release rate.

Another problem with the shear-lag analysis is that it is a one-dimensional analysis and thus can not distinguish between $[0_m/90_n]_s$ and $[90_n/0_m]_s$ laminates. Shear lag analysis predicts that $E_A(\rho)$ is the same for corresponding laminates with the cracked 90° plies in the middle or with the cracked 90° plies on the surfaces. When these identical results for $E_A(\rho)$ are substituted into the appropriate energy release rate results to account for laminate cracking patterns (Equation (3) for $[0_m/90_n]_s$ laminates and Equation (5) for $[90_n/0_m]_s$ laminates), the analysis still does not account for the differences between $[0_m/90_n]_s$ and $[90_n/0_m]_s$ laminates. The results for $[90_n/0_m]_s$ appear to be steeper and to have an intercept at a larger magnitude of ΔT. To generate master plots for all stacking sequences, it is essential to have two-dimensional stress analyses that can distinguish between laminates with microcracking in the middle plies and laminates with

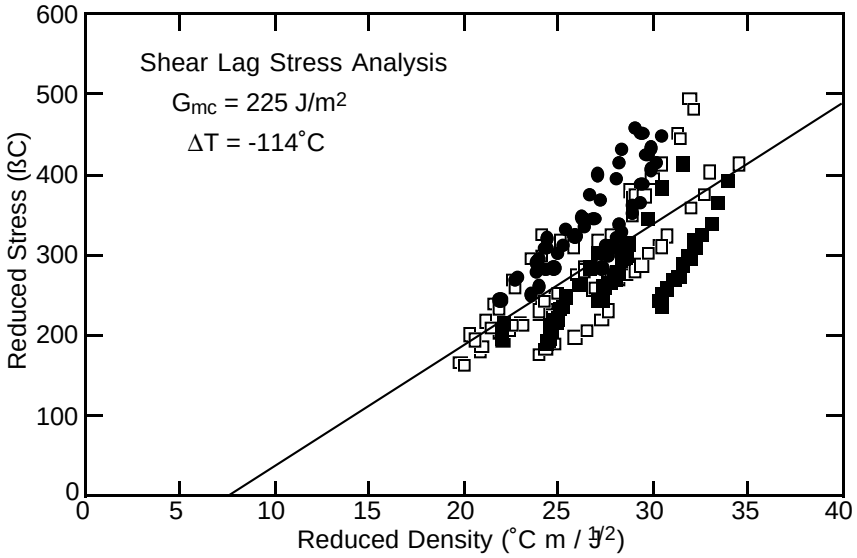

Figure 10 Master plot analysis for 14 $[0_n/90_m]_s$ (open symbols) and $[90_m/0_n]_s$ (filled symbols) AS4/3501-6 carbon/epoxy laminates. $G_{unit}(\rho)$ was calculated from shear-lag analysis with constant displacement boundary conditions. The straight line is a linear fit to the experimental results. The slope and intercept of the fit give $G_{mc} = 225$ J/m^2 and $\Delta T = -114$°C.

staggered microcracks in the surface plies [17].

Master plot analysis of microcracking in laminates reveals two important things. First, finite fracture mechanics of microcracking is an acceptable method for predicting microcracking. Second, the finite fracture mechanics model will not be accurate unless the input stress analysis is for the correct loading conditions and is sufficiently accurate that it gives good results for both $E_A(\rho)$ *and* for the derivative of $E_A(\rho)$. Shear-lag methods are not sufficiently accurate for good microcracking models. In contrast, two-dimensional, variational mechanics methods work well.

One can improve on the variational methods by using refined variational methods [92], averaged upper and lower bound variational analyses [96, 101], multi-layer elasticity methods [106], or even finite element analysis. Although these methods should result in good microcracking models, there is not much room for improvement on the master plot results in Fig. 8. Considering that the complementary energy analysis used for Fig. 8 has an analytical solution [42, 103] while the refined methods require numerical calculations [92, 106], the analytical model may be adequate for interpretation of most microcracking experiments.

Besides numerical complexity, there is another reason not to focus efforts on refined solutions. When such solutions are used to interpret real experiments (*e.g.*, the results in Fig. 8), they typically give worse results than the less accurate complementary energy analysis. A possible explanation for this discrepancy is that the refined solutions all assume a perfect interface between the 0° and the 90° plies. In real materials, the interface is probably not perfect or the formation of a microcrack may slightly damage the interface letting there be slippage between the plies. Slippage could be caused by local delaminations or by matrix plasticity. Analysis of cracking of fibers in the presence of an imperfect interface shows that the energy release rate for cracking is higher when there is interfacial slip than when the interfaces are perfect [96, 98]. Thus, if real materials have interfacial slip, the most accurate elasticity models that do not allow slip will give an energy release rate that is too low. In contrast, the energy release rate calculated by complementary energy gives a rigorous upper bound at low crack density [95, 96] and a practical upper bound at higher crack densities [96]. Perhaps the complementary energy analysis, by giving an energy release rate higher than more accurate methods, fortuitously corrects for some imperfect interface effects in real materials. Improved analysis methods in the future will probably require focusing on experimentally and theoretically accounting for imperfect interface effects.

2.13.3.4 Other Approaches

Although energy methods have mostly replaced strength methods for predicting microcracking, much early work, and some recent work, model microcracking by assuming the next microcrack forms when the stress in the 90° plies reaches the transverse strength, σ_{ult}, of the ply material [2, 25, 20-22, 24-27]. The master plot analysis in the previous section is not limited to energy models; it is also possible to develop a master plot relation for strength models. Plotting microcracking data on a strength-based master plot clearly demonstrates the problems with strength models. In strength models, the next microcrack will form at the location of maximum tensile stress in the 90° plies. Proceeding generically, this maximum stress can be written as:

$$\text{Maximum Stress} = \sigma^0_{xx,1}\sigma^{(max)}_{unit}(\rho) \tag{15}$$

where $\sigma^{(max)}_{unit}(\rho)$ is the maximum tensile stress in a unit cell of damage of aspect ratio ρ when there is unit stress in the 90° plies in the absence of microcracking. $\sigma^{(max)}_{unit}(\rho)$ will change depending on laminate type, but the generic form of the maximum stress will remain the same. A master plot for a strength analysis can be derived be equating maximum stress to σ_{ult}, substituting Equation (9) for $\sigma^0_{xx,1}$, and recasting in the form of Equation (11). The resulting strength master equation is

$$-\frac{k_{m,1}}{k_{th,1}}\sigma_0 = -\frac{\sigma_{ult}}{k_{th,1}\sigma^{(max)}_{unit}(\rho)} + \Delta T \tag{16}$$

A master plot for a strength analysis can be developed by defining a *reduced* stress, σ_R, which is identical to the energy analysis reduced stress (Equation (12)) but a new *reduced* crack density, $D_{R,\sigma}$, as

$$D_{R,\sigma} = -\frac{1}{k_{th,1}\sigma^{(max)}_{unit}(\rho)} \tag{17}$$

A strength criterion predicts that a plot of σ_R as a function of $D_{R,\sigma}$ should be linear. The slope of the plot should be the tensile strength, σ_{ult}, while the intercept should give ΔT. Furthermore, if a strength criterion is valid, the results from a wide variety of laminates should fall on the same straight line or *master plot* for that material.

Figure 11 gives a strength-theory master plot for 14 different laminates of AS4/3501-6 carbon/epoxy laminates. This maximum stress term, $\sigma^{(max)}_{unit}(\rho)$ was calculated using complementary energy methods and variational mechanics [1, 42, 95, 103, 104]. For $[0_n/90_m]_s$ laminates, the maximum stress is midway between the existing microcracks; for $[90_n/0_m]_s$ laminates, the maximum stress occurs at two locations 1/3 and 2/3 of the way between the existing microcracks [1, 17]. The location of the stress maxima accounts for the staggered microcracks in $[90_n/0_m]_s$ laminates (see Fig. 4B). The strength failure criterion leads to a poor master plot. If one examines the results from one laminate, the strength-theory master plot is fairly linear. This observation has mislead some investigators into thinking that strength theories are acceptable. When experiments are done on several laminates of a single type, however, as illustrated in Fig. 11, the results do not converge to a single master plot. Instead, each laminate has its own slope and intercept. In other words, ply strength is not a material property but must be treated as an *in situ* property that depends on laminate structure. Because a strength deduced from one laminate can not be used to predict the microcracking properties of a different laminate of the same material, strength analyses are much less useful than energy analyses. Although the results from different laminates do not lie on a single master plot, it is still possible to do a linear fit to all results. The resulting slope and intercept give unreasonable results. The average slope gives $\sigma_{ult} = 36$ MPa which is too low for the transverse strength of AS4/3501-6 carbon/epoxy laminates. The intercept gives $\Delta T = +85°$C which has the wrong sign for residual stresses that form as the laminate cools from processing temperature to room temperature.

The fit of strength theories to the results for a single laminate can be improved by using statistical methods where the strength is treated as a statistical property [20–24]. But when statistical strength models are applied to a series of laminates for a single material type, they suffer the same fate as simple strength models — the statistical strength parameters are not material properties, but instead must be treated as *in situ* properties that depend on laminate structure [24].

Most statistical models of microcracking are strength models that treat the transverse strength as a statistical parameter. Statistical methods, however, are not confined to strength models. It is also possible

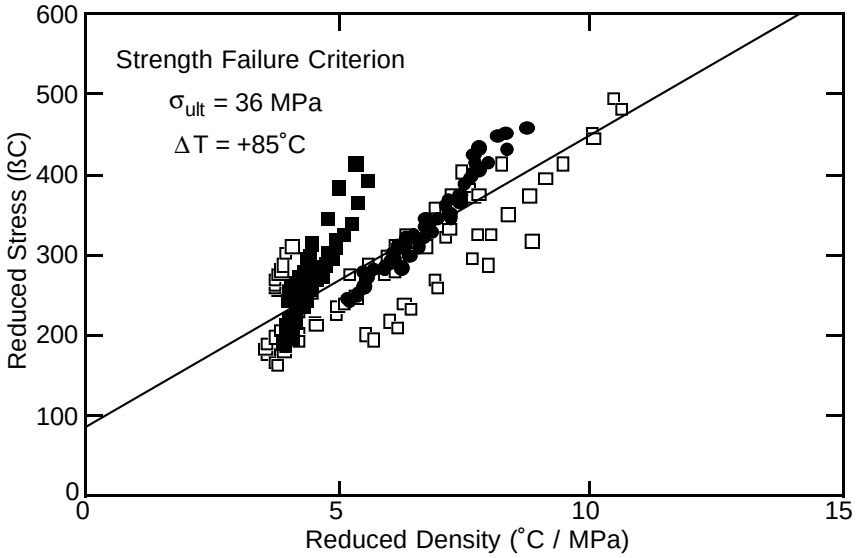

Figure 11 Master plot analysis for 14 $[0_n/90_m]_s$ (open symbols) and $[90_m/0_n]_s$ (filled symbols) AS4/3501-6 carbon/epoxy laminates. $\sigma_{unit}^{(max)}(\rho)$ was calculated from a complementary energy analysis. The straight line is a linear fit to the experimental results. The slope and intercept of the fit give $\sigma_{ult} = 36$ MPa and $\Delta T = +85°$C.

to adjust finite fracture mechanics models of microcracking for statistical effects by letting the microcracking toughness be a statistical parameter. Statistical variations in G_{mc} can by physically justified by noting that 90° plies will invariably have statistical variations in fiber distribution and probably have inherent flaws. It is likely that microcracks will initiate in regions of locally high fiber volume fraction at different loads than at regions of locally low fiber volume fraction. In other words, the microcracking fracture toughness will vary from position to position in the laminate. This variation can be modeled by letting G_{mc} be a statistical quantity.

A statistical fracture mechanics model can be developed by letting G_{mc} follow a Weibull distribution such that the probability of failure of any element of length l_i at applied stress σ_0 becomes

$$P(\sigma_0) = 1 - \exp\left\{-l_i\left(\frac{G_m(\sigma_0)}{G_{m0}}\right)^{\beta}\right\} \tag{18}$$

where $G_m(\sigma_0)$ is the energy released if an element forms a microcrack at applied stress σ_0 and G_{m0} and β are Weibull scale and shape parameters for the laminate toughness. During a statistical microcracking simulation, elements which have not failed at stress σ_0 will have been proof tested to have a toughness greater than the maximum value of $G_m(\sigma_0)$ previously applied to that element (element i) denoted as $G_{max,i}$. Using this extra information, the probability that a *proof-tested* element fails at a subsequent load σ_0 should be determined from the following truncated Weibull distribution:

$$P(\sigma_0) = \begin{cases} 0 & \text{for } G_m(\sigma_0) < G_{max,i} \\ 1 - \exp\left\{-l_i\left[\left(\frac{G_m(\sigma_0)}{G_{m0}}\right)^{\beta} - \left(\frac{G_{max,i}}{G_{m0}}\right)^{\beta}\right]\right\} & \text{for } G_m(\sigma_0) \geq G_{max,i} \end{cases} \tag{19}$$

McCartney [107] has developed a similar statistical simulation of microcracking in which G_{mc} follows a normal distribution instead of Weibull distribution; the results are not significantly different from the simulation results described here.

In brief, to simulate a microcracking experiment with energy as a statistical parameter, a particular laminate is divided into n elements of length l_i and the load is incrementally increased. At each load, $G_m(\sigma_0)$ for formation of a microcrack in each element can be evaluated from the current applied load and the proximity of that element to existing microcracks. To account for the possibility of cracks forming in elements that are not in the middle of a microcracking interval of aspect ratio ρ, Equation (3) can be

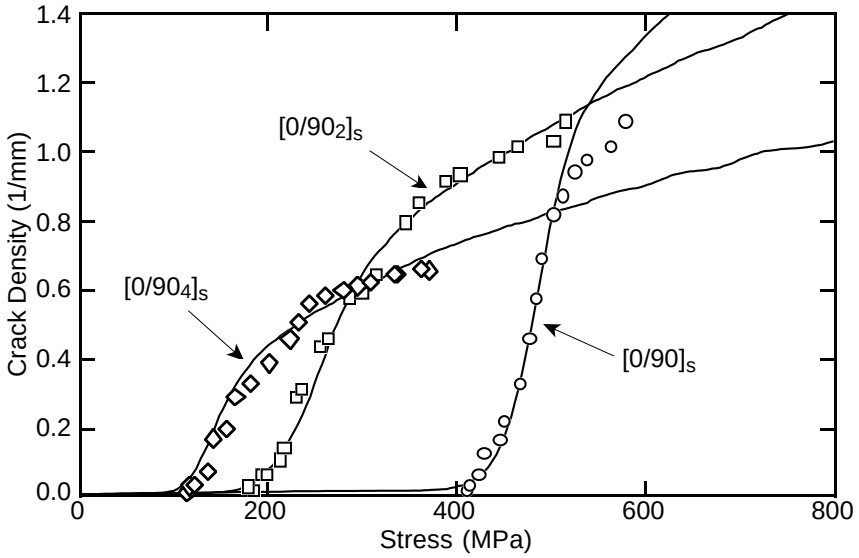

Figure 12 Reanalysis of microcracking experiments on a $[0/90_n]_s$, AS4/3501-6, carbon/epoxy laminate using fracture mechanics but with statistical variations in G_{mc}. The symbols are experimental results. The lines are simulations with G_{mc} described by a Weibull distribution.

generalized to

$$G_m(\sigma_0) = -\frac{1}{2}\rho B\left(\frac{\sigma^0_{xx,1}}{E_{xx,1}}\right)^2\left[\frac{\rho_i E_A(\rho_i) + (\rho-\rho_i)E_A(\rho-\rho_i)}{\rho} - E_A(\rho)\right] \tag{20}$$

where ρ_i is the distance from element i to one of the neighboring cracks. Once $G_m(\sigma_0)$ is known, it can be substituted into Equation (19) and compared to a random number to decide if that element should crack during the current loading step. The simulation is continued until many cracks form. Averaging several such simulations gives a prediction for crack density as a function of applied load that can be compared to experimental results.

The results of a microcracking simulation with G_{mc} as a statistical parameter for the three AS4/3501-6, carbon/epoxy laminates previously presented in Fig. 2 are given in Fig. 12. The simulation curves were generated by dividing the laminate into 1000 elements and averaging the results of 30 simulations. The Weibull scale and shape parameters were adjusted to fit experimental results. All three laminates could be fit with similar parameters, but the best fits for each required slightly different parameters. The statistical simulations completely resolve the two discrepancies discussed above between experimental results and finite fracture mechanics predictions with a single value for G_{mc}. First, the statistical simulations correctly reproduces the initial slow rise in microcrack density. It was previously argued that this slow rise is caused by statistical inhomogeneities or flaws in the laminate. The statistical simulation accounts for these homogeneities and reproduces the experimental results. Second, the fits in Fig. 2 had to be corrected at high crack density to account for new cracks forming in microcrack intervals that are larger than the average microcrack interval. The statistical simulation automatically simulates a distribution in microcrack interval sizes with new microcracks being more likely to form in the larger crack intervals. The simulation thus fits the high crack density data without any corrections. The main use of the statistical simulation is that it resolves all discrepancies between simpler predictions and experimental results. In practical terms, however, it is less useful. Experimental data can be fit by adjusting Weibull parameters G_{m0} and β. The results, however, are relatively insensitive to β. In other words, it is not possible to accurately determine β from microcracking data. All that can be determined is the Weibull scale parameter G_{m0}. After suitable correction of length units, this scale parameter gives essentially the same information as G_{mc} from fits such as those in Fig. 2.

2.13.3.5 Effective Laminate Properties

One detrimental effect of microcracks is that they cause the effective thermomechanical properties of the laminate to change. When one is designing for applications that might develop microcracking before final failure, it is important to know how laminate properties are changed and therefore to assess if designs can survive the presence of some level of microcracking. A general microcracked laminate can be represented as an orthotropic plate with 12 effective material properties. Here we take x as the direction of the fibers in the 0° plies, y as the direction of the fibers in the 90° plies and z as the thickness direction. The twelve independent effective thermomechanical properties that depend on crack density ρ are three tensile moduli ($E_{xx}(\rho)$, $E_{yy}(\rho)$, and $E_{zz}(\rho)$), three shear moduli ($G_{xy}(\rho)$, $G_{xz}(\rho)$, and $G_{yz}(\rho)$), three Poisson ratios ($\nu_{xy}(\rho)$, $\nu_{xz}(\rho)$, and $\nu_{yz}(\rho)$), and three thermal expansion coefficients ($\alpha_{xx}(\rho)$, $\alpha_{yy}(\rho)$, and $\alpha_{zz}(\rho)$).

A prerequisite of deriving the finite fracture mechanics analysis of microcracking is the derivation of an accurate analysis for $E_A(\rho)$. In fact, all energy release rate results were shown to depend only on $E_A(\rho)$. In the $x-y-z$ coordinates, $E_A(\rho)$ is $E_{xx}(\rho)$. It has recently been shown, that once $E_{xx}(\rho)$ is known, most other effective properties can be calculated without any additional analyses [107–109]. The key results were derived by McCartney [107, 108]; he was able to derive the following exact relations between effective thermomechanical properties and the damage function defined in Equation (7):

$$\frac{\nu_{xy}}{E_{xx}} - \frac{\nu_{xy}(\rho)}{E_{xx}(\rho)} = k\Phi(\omega) \tag{21}$$

$$\frac{1}{E_{yy}(\rho)} - \frac{1}{E_{yy}} = k^2\Phi(\omega) \tag{22}$$

$$\frac{\nu_{xz}}{E_{xx}} - \frac{\nu_{xz}(\rho)}{E_{xx}(\rho)} = k'\Phi(\omega) \tag{23}$$

$$\frac{1}{E_{zz}(\rho)} - \frac{1}{E_{zz}} = (k')^2\Phi(\omega) \tag{24}$$

$$\frac{\nu_{yz}}{E_{yy}} - \frac{\nu_{yz}(\rho)}{E_{yy}(\rho)} = kk'\Phi(\omega) \tag{25}$$

$$\alpha_{xx}(\rho) - \alpha_{xx} = k_1\Phi(\omega) \tag{26}$$

$$\alpha_{yy}(\rho) - \alpha_{yy} = kk_1\Phi(\omega) \tag{27}$$

$$\alpha_{zz}(\rho) - \alpha_{zz} = k'k_1\Phi(\omega) \tag{28}$$

where properties without (ρ) are properties of the undamaged laminate and the constants k, k', and k_1 are constants that depend only on the properties of the undamaged laminate [107, 108]. These relations show that all effective tensile moduli, Poisson ratios, and thermal expansion coefficients can be determined once $E_{xx}(\rho)$ is known. The shear moduli are not covered by these relations and thus their analysis requires separate mechanics analyses. One method of determining effective shear modulus of cracked lamina by variational mechanics has been described by Hashin [103]. Finally, all these effective property results are limited to laminates in which only plies of a single orientation are cracked. The analysis is aimed at laminates in which only the 90° plies are cracked, but it can easily be extended to plies of a different angle being cracked by rotation of the coordinate system and the effective properties such that the cracked plies become 90° plies. The analysis does not predict effective properties of laminates in which multiple plies of different angles in the same laminate are cracked. For example, If θ is not too large, $[0/\theta/-\theta]_s$ or $[0/\theta/-\theta/90]_s$ laminates can develop microcracks in the θ, $-\theta$, and 90° plies. The effective property analysis of laminates with multiple, microcracked plies requires analysis by alternative methods.

2.13.4 APPLICATION OF MICROCRACKING EXPERIMENTS TO MATERIAL ISSUES

2.13.4.1 Microcracking Fracture Toughness

Experiments that measure microcrack density as a function of applied load can be fit using a finite fracture mechanics analysis to determine G_{mc}. This composite toughness property can be studied by itself as a

Table I The microcracking fracture toughness of several composite material systems. All G_{mc} values have been derived by a finite fracture mechanics analysis with $E_A(\rho)$ calculated by variational mechanics.

Composite Material	G_{mc} (J/m^2)	References
E-Glass/Epoxy	200	[14,90]
AS4/Hercules 3501-6	220–260	[41,42]
IM7/FIberite 954-2A	240	[72]
AS4/Dow Polycyanate	430–460	[40]
AS4/Polysulfone	450	[72]
IM7/Hecules 8551-7	525	[40]
AS4/Dow Tactix® 556	550	[40]
Scotch Ply 1003 (E-Glass/Epoxy)	650	[122]
T300/Fiberite 934	690	[41]
G40-800/rubber modified Dow Polycyanate	720	[40]
AS4/Dow Tactix® 696	825	[40]
IM6/DuPont Avimid® K Polymer	960	[41,70-72]
IM7/PETI5	1080	[71]
T300/Fiberite 977-2	1800-2400	[41]
AS4/ICI PEEK	3000	[41]

measure of the resistance of a given material to the development of microcracks. Table I lists a number of composite material systems that have been subjected to microcracking experiments and analyzed using methods similar to those discussed in this chapter. Thermoset matrix composites have lower toughnesses (*e.g.*, AS4/Hercules 3501-6); thermoplastic matrix composites can have G_{mc} of 1000 J/m^2 or higher (*e.g.*, IM7/PETI5 and AS4/ICI PEEK). Glass fiber composites have similar microcracking toughnesses to carbon fiber composites. Although thermoplastic-matrix composites have higher microcracking toughness than thermoset-matrix composites, they also have higher levels of residual thermal stresses [118, 119]. Because the residual stresses in the 90° plies are tensile stresses, a higher level of residual stresses promotes microcracking. Combining the effects of higher toughness and higher residual stresses, the stress to form microcracks is not significantly different between thermoset- and thermoplastic-matrix composites.

Because microcrack growth is mode I crack growth parallel to the fibers, it might be expected to be similar to the mode I delamination toughness of the same material, . Delamination toughness is usually measured by conventional fracture mechanics experiments on double cantilever beam specimens made from unidirectional composites [121]. When G_{Ic} is compared to G_{mc}, the general trend as that composites with brittle matrices tend to have a higher G_{mc} than G_{Ic}, while composites with tougher matrices tend to have a lower G_{mc} than G_{Ic}. In other words, the variation in G_{mc} for a range of matrices is smaller than the variation in G_{Ic}. The crack front for microcrack propagation is normal to the ply faces while the crack front for delamination is parallel to the ply faces. Although they are both crack growth parallel to the fibers, they may be measuring different material properties — G_{Ic} is measuring *interlaminar* toughness while G_{mc} is measuring *intralaminar* toughness. Although there are few results in the literature, it is also possible to do standard fracture mechanics experiments on unidirectional composites with the crack front normal to the ply faces [42, 120]. When G_{mc} and intralaminar fracture experiments were done on the same material system, G_{mc} was found to be very close to intralaminar toughness [42].

2.13.4.2 G_{mc} as a Material Probe

Because the first form of failure in composites containing 90° plies is microcracking in those plies, changes in the microcracking properties of a laminate can be used as a sensitive probe to changes in the failure properties of the laminate. Such experiments have been used to monitor physical aging [72], hygrothermal stability [70, 71], and thermal degradation [122]. In brief, a series of laminates can be subjected to any

specified conditions for various amounts of time. For each time period, some laminates can be removed and subjected to standard microcracking experiments to determine G_{mc}. Changes in G_{mc} can be used to study the effect of the selected conditions on composite failure properties. For many conditions, the changes in G_{mc} will be much more dramatic than changes in other lamina properties [70, 71, 72]. Thus G_{mc} can be a sensitive probe for monitoring changes in laminate properties. This section gives one example which used G_{mc} to study the hygrothermal stability of polyimide composites [70, 71].

When studying the durability of polyimide-matrix, carbon-fiber composites, it was observed that cross-ply and quasi-isotropic laminates immersed in 80°C water would spontaneously develop microcracks in the 90° plies [70]. The implication was that the microcracking toughness or G_{mc} drops during hot-wet conditions and that microcracks form once G_{mc} drops sufficiently low that microcracks can form due to residual stresses alone. The durability issues raised by spontaneous microcracking could be studied by continued long-term exposure experiments. Such experiments, however, would be time consuming because there was no apparent change in the laminates until the formation of cracks which took more than 500 hours to form [70]. Because G_{mc} is a sensitive measure of laminate failure properties, studies on the drop in G_{mc} might reveal information on degradation more quickly and give more information for studying the kinetics of degradation. Indeed, spontaneous microcracking must be accompanied by very large drops in G_{mc}. The spontaneous microcracks form by residual stresses alone, but the both the hot (closer to the stress-free temperature) and wet (moisture-induced swelling reduces thermal shrinkage-induced stresses) conditions should reduce residual stresses — G_{mc} must be dropping to almost zero prior to spontaneous microcracking.

Figure 13 shows the microcracking toughness of Avimid®K Polymer/IM7 laminates as a function of time during exposure to various levels of humidity at 80°C [70, 71]. After each exposure time, the $[0/90_2]_s$ laminates were removed and redried before doing microcracking experiments such as those in Fig. 2. Thus changes in G_{mc} could be compared to the initial G_{mc} to monitor changes in laminate failure properties. When immersed in water (100%), G_{mc} drops rapidly and becomes nearly zero in about 500 hours. At lower humidity (76% and 50%), the toughness drops at a lower rate. At the lowest humidity (26%), the toughness did not drop during the time interval studied. Because the amount of water absorbed is proportional to the humidity, the results at reduced humidity suggest there may be a threshold level of water below which no degradation occurs. The results at 26% humidity never reached the threshold level and thus do not degrade. Similarly, the results at 50% humidity took longer to reach the threshold level than the higher humidity results which could account for the delay of about 200 hours before degradation began. This idea was used to suggest a simple first-order-kinetics, hydrolysis analysis in which the rate of degradation was assumed to be proportional to the total water-absorption concentration, $[H_2O](t)$, above some threshold water concentration, $[H_2O]_{thres}$. This simple kinetics analysis integrates to:

$$G_{mc}(t) = \begin{cases} G_{mc}^0 & \text{for } t < t_{thres} \\ G_{mc}^0 e^{-k\int_{t_{thres}}^{t}([H_2O](t)-[H_2O]_{thres})dt} & \text{for } t > t_{thres} \end{cases} \tag{29}$$

where t_{thres} is the time to reach the threshold water concentration and G_{mc}^0 is the toughness before exposure. The results of experiments at several humidities and several temperatures could all be fit Equation (29); k and $[H_2O]_{thres}$ depend on temperature, but are independent of humidity at constant temperature [71].

By Equation (29), any specimen that has been exposed to the same integrated water exposure (the power of the exponential) should have the same degradation in G_{mc}. This observation makes it possible to derive an effective time analysis for construction of a master plot for degradation at any reference temperature and humidity. For example, for reference conditions of 80°C and immersed, the effective time under reference conditions, t_{eff}, is defined by the integral equation

$$\int_{t_{thres,ref}}^{t_{eff}} k(T_{ref})([H_2O](t) - [H_2O]_{thres,ref})dt = \int_{t_{thres}}^{t} k(T)([H_2O](t) - [H_2O]_{thres})dt \tag{30}$$

where $t_{thres,ref}$, $k(T_{ref})$, and $[H_2O]_{thres,ref}$ describe the degradation kinetics under reference conditions and t_{thres}, $k(T)$, and $[H_2O]_{thres}$ are for any other conditions. Equation (30) can be solved numerically, or analytically (with some simple approximations [71]) to convert all results to reference conditions. Such a master-plot for degradation of Avimid® K polymer laminates is given in Fig. 14. The results for several different humidities and several different temperatures all scale to the same master plot. Thus monitoring

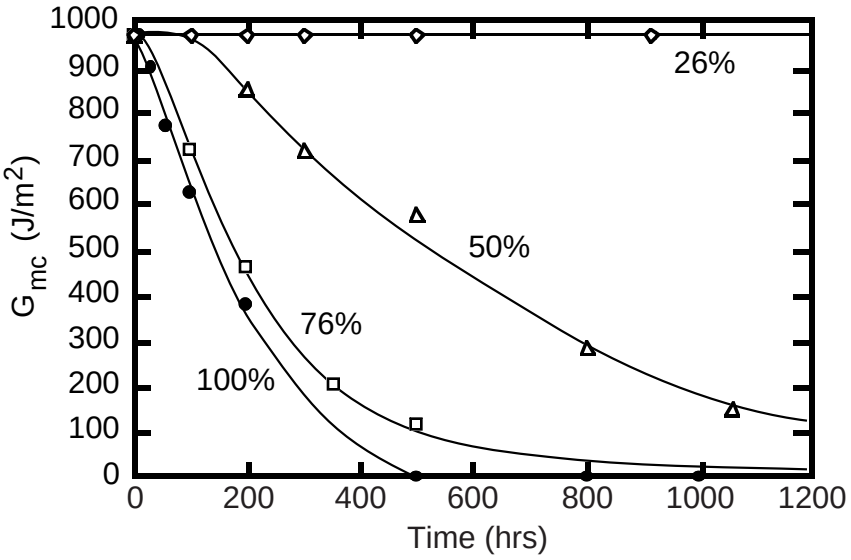

Figure 13 Microcracking fracture toughness, G_{mc}, as a function of time for Avimid® K polymer laminates aged at 80°C while immersed in water (100%) or exposed to relative humidities of 76%, 50%, and 26%.

G_{mc} is useful for probing the kinetics of hygrothermal stability of composite materials. It allows one to observe changes in laminate properties before other changes, such as spontaneous microcracks, occur. The possibility of a master plot also provides an accelerated test method. By converting the master plot results to any other reference conditions using Equation (30) it should be possible to predict hygrothermal stability at any temperature and humidity for which the master plot is valid.

2.13.4.3 Fatigue Experiments

Finite fracture mechanics analysis of microcracking can also be used to interpret mechanical fatigue [1, 12, 13, 14, 32, 35, 38, 58, 74–84,123], thermocycling fatigue [1, 16, 55, 56, 57, 58, 66–69, 85, 86], and combined

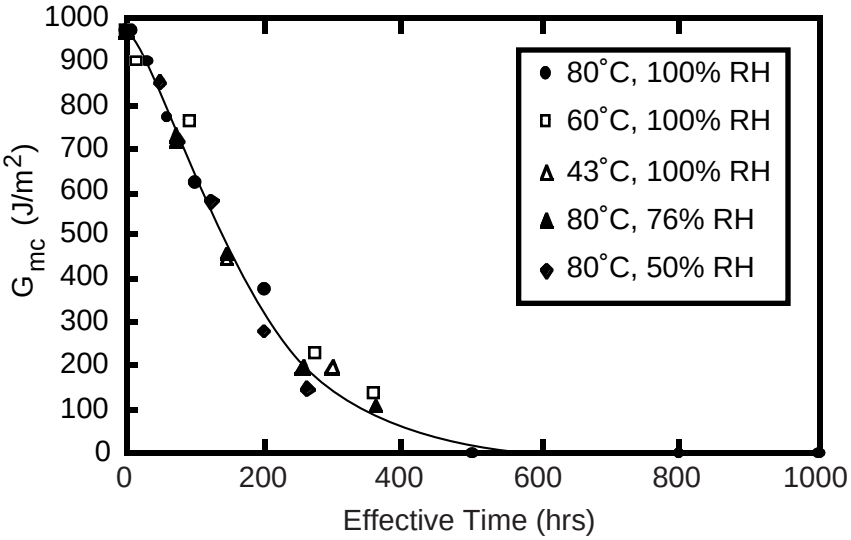

Figure 14 Master plot for hygrothermal aging of Avimid® K polymer laminates for reference conditions of immersion in water at 80°C

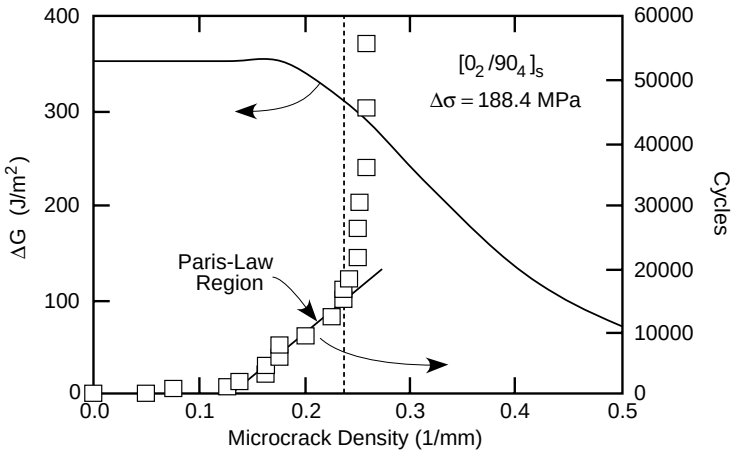

Figure 15 Microcracking fatigue data for a $[0_2/90_4]_s$ carbon/epoxy laminate. The solid line shows ΔG as a function of microcrack density. The symbols show the microcrack density as a function of cycle number. The straight line through the microcrack density data shows the Paris-law region of constant microcrack density growth rate.

thermal and mechanical fatigue [16, 124]. Conventional fracture mechanics analysis of fatigue crack growth normally uses a Paris law [125] in which the crack growth rate is related to the range in applied stress intensity factor by a power law:

$$\frac{da}{dN} = A\Delta K^n \tag{31}$$

In microcracking, there is no observation of crack growth, but it is possible to measure the rate of increase in crack density per cycle or dD/dN. There is also no crack tip stress intensity factor, but one can calculate the range in microcracking energy release rate, ΔG_m, during any thermomechanical cycling using, for example, Equation (4). When these two observations are combined in a modified Paris law of

$$\frac{dD}{dN} = A\Delta G_m^n \tag{32}$$

it is found that results for several different laminates of the same material can be correlated on a single master Paris law plot [1, 15, 16, 124]. The use of Equation (32) can be supported by experimental results, such as those in Fig. 15, for crack density, D, as a function of cycle number, N. These results are for microcracking of a $[0_2/90_4]_s$ carbon/epoxy laminate with a constant stress amplitude. The smooth curve is a calculation of ΔG_m using Equation (4). A property of ΔG_m under load control is that it is constant at low crack density when there are no interactions between cracks. At higher crack density the cracks begin to interact and the total energy released by each new microcrack decreases. By Equation (32) the constant ΔG_m at low crack density should yield a constant dD/dN. Initially, however, the increase in crack density is very fast and not constant (up to 0.1 mm^{-1}). These early cracks have been attributed to flaws [15, 16] just as were the first few points in microcrack density *vs.* applied load experiments that cause deviations between theory and experiments (see Fig. 2). After the first few microcracks, the crack density increases linearly as long as ΔG_m remains nearly constant. The slope of this linear region gives dD/dN for the constant ΔG_m from the applied load amplitude. At high crack density, ΔG_m decreases and in agreement with Equation (32), that drop causes the dD/dN to drop.

To generate a Paris law plot for a given material, one can do a series of experiments such as illustrated in Fig. 15, for a variety of laminates and a variety of stress amplitudes. Cross plotting the slope of the Paris-law region as a function of the calculated ΔG_m gives a microcracking fatigue resistance plot; by Equation (32), this plot should be linear with slope n. Some sample experimental results for Avimid® K Polymer laminates are given in Fig. 16. Most of the plot is linear. Furthermore, the results from different layups fall on the same line which further demonstrates the ability of the finite fracture mechanics analysis of microcracking to correlate microcracking results. The earliest and latest points deviate from the line. The result at high ΔG_m is close to the static toughness of these laminates and thus microcracking occurs in a single cycle. The point

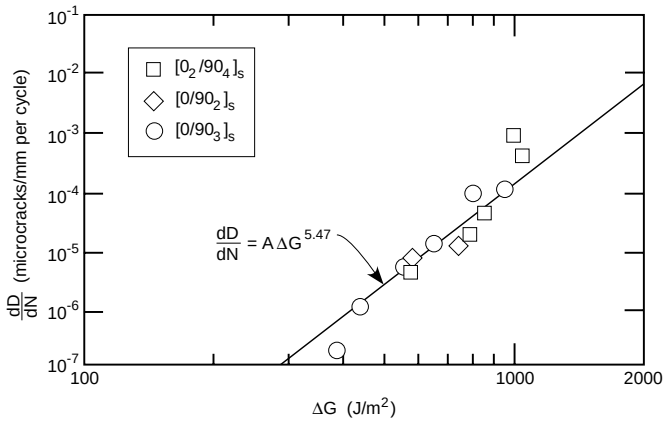

Figure 16 The microcrack density growth rate (in microcracks per mm per cycle) as a function of applied ΔG for Avimid® K Polymer/IM6 laminates. As indicated on the figure, the results are from three different cross-ply layups.

at the lowest ΔG_m hints at a threshold limit below which microcracks will not form. More experimental results would be needed to confirm threshold effects.

If unloaded laminates are thermocycled between temperatures T_{low} and T_{high}, it is possible to derive a ΔG_m due to residual stresses alone. From the load-control result in Equation (4), the microcrack driving force during thermocycling can be found from:

$$\Delta G_m = \frac{1}{2}\rho B \left(\frac{E_{A0}}{E_{xx,1}}\right)^2 k_{th,1}^2 \left[(T_{low} - T_0)^2 - (T_{high} - T_0)^2\right] \left[\frac{1}{E_A(\rho/2)} - \frac{1}{E_A(\rho)}\right] \tag{33}$$

where T_0 is the stress-free temperature. Note that the maximum G_m occurs at low temperature and thus thermocycling experiments are for formation of microcracks at T_{low}. A Paris-law plot for a series of thermocycling experiments conducted exactly like the mechanical fatigue tests is given in Fig. 17. By using finite fracture mechanics to calculate ΔG_m, it is possible the correlate the results for six different laminates and over two different temperature ranges on the same microcracking fatigue resistance plot; the plot is linear which matches the modified Paris law in Equation (32). The calculation in Equation (33) assumes that the thermomechanical properties of the laminate are independent of temperature over the temperature range of the thermocycling. If the properties depend on temperature, those effects should be included in the calculation of ΔG_m.

The modified Paris law in Equation (32) suggests that ΔG_m is the only controlling parameter. In principal, it should be possible to correlate mechanical fatigue experiments with thermocycling experiments and with combined thermo-mechanical fatigue cycling. Such a correlation normally does not work because there are temperature effects on the material that cause the damage processes during constant-temperature mechanical tests to differ from those during variable-temperature thermocycling. These effects are not simply the difference in temperature at the point of crack formation. The microcracks should form at the point of maximum G_m which occurs at maximum stress during mechanical fatigue and at minimum temperature (or maximum $|\Delta T|$) during thermal cycling. If the temperature at the point of formation was the only difference in damage processes, thermocycling results should correlate with low-temperature mechanical fatigue results. The experimental observation, however, is that that are still differences between thermocycling results and low-temperature mechanical fatigue results [16, 124].

During high-cycle fatigue experiments it is possible to observe microcracks initiating on the edge and propagating across the width of the laminate [32, 35, 38, 79]. With such observations, it is possible to do conventional fatigue crack propagation experiments. The experiments are to record microcrack length as a function of cycle number. The observations of many cracks suggest that crack growth rate is independent of crack length and only a function of the distance to the pre-existing neighboring microcracks. By the modified Paris law, this result suggests that $G(a, \rho)$, or the energy release rate as a function of microcrack length, is independent of a and only a function of the crack interval size, ρ, where the crack is growing. The calculations for finite fracture mechanics of microcracking only seeks to find the *total* change in energy for

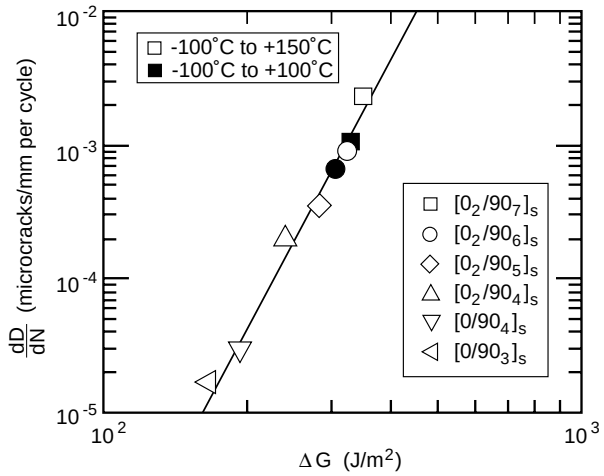

Figure 17 The microcrack density growth rate (in microcracks/mm per cycle) as a function of applied ΔG for AS4/Hercules 3501-6 during thermal cycling. As indicated on the figure, the results are from six different cross-ply layups and from two different thermal cycling temperature ranges.

formation of a complete microcrack in a crack interval of size ρ. This total energy is related to an integration of $G(a, \rho)$ by:

$$G_m(\rho) = \frac{1}{W} \int_0^W G(a, \rho)\, da \tag{34}$$

From the fatigue observation that $G(a, \rho)$ is independent of a, it can come out of the integral to give:

$$G(a, \rho) = G_m(\rho) \tag{35}$$

Thus, the driving force for individual microcrack propagation, $G(a, \rho)$, can be calculated from finite fracture mechanics calculations of $G_m(\rho)$. Such methods have been used to interpret microcrack propagation results during fatigue [32, 35, 38, 79].

2.13.5 SUMMARY

Matrix microcracking is a very common damage mode in composite laminates. Because microcracks cause degradation in properties and act as precursors to other forms of damage leading to laminate failure, it is important for anyone designing with composites to have a basic understanding of microcracking processes. The goal of this chapter has been summarize experimental observations about microcracking and to offer a fracture mechanics or energy analysis method as a tool for understanding and predicting microcracking under a variety of conditions. The energy analysis can correlate most experimental results. In static tests, a given material can be characterized by a microcracking fracture toughness, G_{mc}. Once G_{mc} is known, the microcracking properties of any laminate constructed from that material can be predicted. An energy analysis with a single-valued G_{mc} misses a few second-order effects in experimental results. More refined analyses accounting for such things as statistical variations in G_{mc} and imperfect interface effects between the cracking plies and the supporting plies already can, or can be developed to, explain the missed second-order effects. In other words, existing energy models capture perhaps 90% of experimental observations. If necessary, and it will probably not be necessary for very many applications, refined models can capture the remaining 10% of experimental observations. The fracture mechanics methods can be extended to help understand mechanical fatigue and thermocycling results as well. This chapter has dealt only with laminates having cracks in 90° plies. The fracture mechanics principles should be applicable to more general microcracking damage processes. The application of those principles, however, will require new stress analyses and energy release rate calculations for more general damage patterns. In summary, the concept that microcracks form

when the energy released by that fracture event exceeds some critical value is an underlying principle that can tie together existing experimental results and provide a starting point for analyzing microcracking under new loading or environmental conditions.

2.13.6 REFERENCES

1. J. A. Nairn and S. Hu, Micromechanics of Damage: A Case Study of Matrix Microcracking. In *Damage Mechanics of Composite Materials*, ed., Ramesh Talreja, Elsevier, Amsterdam (1994) 187–243.
2. K. W. Garrett and J. E. Bailey, Multiple Transverse Fracture in 90° Cross-Ply Laminates of a Glass Fibre-Reinforced Polyester. *J. Mat. Sci* **12** (1977) 157–168.
3. K. W. Garrett and J. E. Bailey, The Effect of Resin Failure Strain on the Tensile Properties of Glass Fiber-Reinforced Cross-Ply Laminates.. *J. Mat. Sci.* **12** (1977) 2189–2194.
4. A. Parvizi, K. W. Garrett, and J. E. Bailey, Constrained Cracking in Glass Fiber-Reinforced Epoxy Cross-Ply Laminates. *J. Mat. Sci.* **13** (1978) 195–201.
5. M. G. Bader, J. E. Bailey, P. T. Curtis, and A. Parvizi, The Mechanisms of Initiation and Development of Damage in Multi-Axial Fibre-Reinforced Plastics Laminates.. *Proc. 3rd Int'l Conf. on Mechanical Behavior of Materials* **3** (1979) 227–239.
6. J. E. Bailey, P. T. Curtis and A. Parvizi, On the Transverse Cracking and Longitudinal Splitting Behavior of Glass and Carbon Fibre Epoxy Cross-Ply Laminates and the Effect of Poisson and Thermally Generated Strains. *Proc. R. Soc. Lond. A* **366** (1979) 599–623.
7. J. E. Bailey and A. Parvizi, On Fiber Debonding Effects and the Mechanism of Transverse-Ply Failure in Cross-Ply Laminates of Glass/Fiber/Thermoset Composites. *J. Mat. Sci.* **16** (1981) 649–659.
8. F. R. Jones, A. R. Wheatley, and J. E. Bailey, The Effect of Thermal Strains on the Microcracking and Stress Corrosion Behavior of GRP. In *Composite Structures*, ed., I. H. Marshall, Appl. Sci. Publ, Barking, UK (1981) 415–429.
9. H. T. Hahn and S. W. Tsai, On the Behavior of Composite Laminates After Initial Failures. *J. Comp. Mat.* **8** (1974) 288–305.
10. S. W. Tsai and E. M. Wu, A General Theory of Strength for Anisotropic Materials. *J. Comp. Mater.* **5** (1971) 58–80.
11. D. L. Flaggs and M. H. Kural, Experimental Determination of the In Situ Transverse Lamina Strength in Graphite/Epoxy Laminates. *J. Comp. Mat.* **16** (1982) 103–115.
12. J. Tong, F. J. Guild, S. L. Ogin, and P. A. Smith, On Matrix Crack Growth in Quasi-Isotopic Laminates - I. Experimental Investigation. *Comp. Sci. & Tech.* **57** (1997) 1527–1535.
13. W. W. Stinchcomb, K. L. Reifsnider, P. Yeung, and J. Masters, Effect of Ply Constraint on Fatigue Damage Development in Composite Material Laminates. *ASTM STP* **723** (1981) 64–84.
14. A. L. Highsmith and K. L. Reifsnider, Stiffness-Reduction Mechanisms in Composite Laminates. *ASTM STP* **775** (1982) 103–117.
15. J. A. Nairn, S. Hu, S. Liu, and J. S. Bark, The Initiation, Propagation, and Effect of Matrix Microcracks in Cross-Ply and Related Laminates. *Proc. of the* 1^{st} *NASA Advanced Composite Tech. Conf.* **Seattle, WA, Oct. 29 to Nov. 1, 1990** (1990).
16. J. A. Nairn, Microcracking, Microcrack-Induced Delamination, and Longitudinal Splitting of Advanced Composite Structures. *NASA CR 4472* (1992).
17. J. A. Nairn and S. Hu, The Formation and Effect of Outer-Ply Microcracks in Cross-Ply Laminates: A Variational Approach. *Eng. Fract. Mech.* **41** (1992) 203–221.
18. L. Berglund and J. Varna, Transverse Cracking and Local Delamination in $[0_4/90_n]_s$ and $[90_n/0_4]_s$ Carbon Fiber/Toughened Epoxy Laminates. *J. Reinf. Plast. & Comp.* **11** (1992) 643–660.
19. P. A. Smith, L. Boniface, and N. F. C. Glass, A Comparison of Transverse Cracking Phenomena in $(0/90)_s$ and $(90/0)_s$ CFRP Laminates. *Appl. Comp. Mater.* **5** (1998) 11–23.
20. H. Fukunaga, T. W. Chou, P. W. M. Peters, and K. Schulte, Probabilistic Failure Strength Analysis of Graphite/Epoxy Cross-Ply Laminates. *J. Comp. Mat.* **18** (1984) 339–356.
21. H. Fukunaga, T. W. Chou, K. Schulte, and P. W. M. Peters, Probabilistic Initial Failure Strength of Hybrid and Non-Hybrid Laminates. *J. Mat. Sci.* **19** (1984) 3546–3553.

22. P.W.M. Peters, The Strength Distribution of 90° Plies in 0/90/0 Graphite-Epoxy Laminates. *J. Comp. Mat.* **18** (1984) 545–556.
23. N Takeda and S. Ogihara, In Situ Observation and Probabilistic Prediction of Microscopic Failure Processes in CFRP Cross-Ply Laminates. *Comp. Sci. & Tech.* **52** (1994) 183–195.
24. P. W. M. Peters, The Fibre/Matrix Bond Strength of CFRP Deduced from the Strength Transverse to the Fibres. *J. Adhesion* **53** (1995) 79–100.
25. A. Parvizi and J. E. Bailey, On Multiple Transverse Cracking in Glass-Fiber Epoxy Cross-Ply Laminates. *J. Mat. Sci.* **13** (1978) 2131–2136.
26. F. W. Crossman, W. J. Warren, A. S. D. Wang, and G. E. Law, Jr., Initiation and Growth of Transverse Cracks and Edge Delamination in Composite Laminates: Part 2. Experimental Correlation. *J. Comp. Mat Supplement* **14** (1980) 89–108.
27. P. W. Manders, T. W. Chou, F. R. Jones, and J. W. Rock, Statistical Analysis of Multiple Fracture in [0/90/0] Glass fiber/epoxy resin laminates. *J. Mat. Sci.* **19** (1983) 2876–2889.
28. A. S. D. Wang, Fracture Mechanics of Sublaminate Cracks in Composite Materials. *Comp. Tech. Rev.* **6** (1984) 45–62.
29. R. Jamison, K. Schulte, K. L. Reifsnider, and W. W. Stinchcomb, Characterization and Analysis of Damage Mechanisms in Tension-Tension Fatigue of Graphite/Epoxy Laminates. *ASTM STP* **836** (1984) 21–55.
30. A. S. D. Wang, N. N. Kishore and C. A. Li, Crack Development in Graphite-Epoxy Cross-Ply Laminates under Uniaxial Tension. *Comp. Sci. & Tech.* **24** (1985) 1–31.
31. A. S. D. Wang, Fracture Analysis of Matrix Cracking in Laminated Composites. *Naval Air Development Center Report No. NADC 85118-60* (1985) 1–161.
32. M. G. Bader and L. Boniface, Damage Development During Quasi-Static and Cyclic Loading in GRP and CFRP Laminates Containing 90 Plies.. *Proc.* 5^{th} *Int'l Conf. on Comp. Mat.* **San Diego, CA, July 29-August 1** (1985) 221–232.
33. M. Caslini, C. Zanotti, and T. K. O'Brien, Fracture Mechanics of Matrix Cracking and Delamination in Glass/Epoxy Laminates. *J. Comp. Tech & Research* **Winter** (1987) 121–130.
34. S. E. Groves, C. E. Harris, A. L. Highsmith, and R. G. Norvell, An Experimental and Analytical Treatment of Matrix Cracking in Cross-Ply Laminates. *Experimental Mechanics* **March** (1987) 73–79.
35. L. Boniface, P. A. Smith, S. L. Ogin, and M. G. Bader, Observations on Transverse Ply Crack Growth in a $[0/90_2]_s$ CFRP Laminate Under Monotonic and Cyclic Loading. *Proc* 6^{th} *Int'l Conf. on Comp. Mat.* **3** (1987) 156–165.
36. Y. M. Han, H. T. Hahn, and R. B. Croman, A Simplified Analysis of Transverse Ply Cracking in Cross-Ply Laminates. *Comp. Sci. & Tech.* **31** (1987) 165–177.
37. N. Laws and G. J. Dvorak, Progressive Transverse Cracking in Composite Laminates. *J. Comp. Mat.* **22** (1988) 900–916.
38. L. Boniface and S. L. Ogin, Application of the Paris Equation to the Fatigue Growth of Transverse Ply Cracks. *J. Comp. Mat.* **23** (1989) 735–754.
39. K. C. Jen and C. T. Sun, Matrix Cracking and Delamination Prediction in Graphite/Epoxy Laminates. *Proc. of the Amer. Soc. Comp,* 5^{th} *Tech. Conf.* (1990) 350–360.
40. S. Yalvac, L. D. Yats, and D. G. Wetters, Transverse Ply Cracking in Toughnened and Untoughened Graphite/Epoxy and Graphite/Polycyanate Crossply Laminates. *J. Comp. Mat.* **25** (1991) 1653–1667.
41. S. Liu and J. A. Nairn, The Formation and Propagation of Matrix Microcracks in Cross-Ply Laminates During Static Loading. *J. Reinf. Plast. & Comp.* **11** (1992) 158–178.
42. J. A. Nairn, S. Hu, and J. S. Bark, A Critical Evaluation of Theories for Predicting Microcracking in Composite Laminates. *J. Mat. Sci.* **28** (1993) 5099–5111.
43. H. L. McManus and J. R. Maddocks, On Microcracking in Composite Laminates Under Thermal and Mechanical Loading. *Polymers & Polymer Composites* **4** (1996) 305–314.
44. Y. C. Michii and H. L. McManus, Prediction of Microcracking Distribution in Composite Laminates Using a Monte-Carlo Simulation Method. *J. Reinf. Plast. & Comp.* **16** (1997) 1220–1230.
45. Y. Leterrier, L. Boogh, J. Andersons, and J.-A. E. Manson, Adhesion of Silicon Oxide Layers on

Poly(ethylene terepthalate). I: Effect of Substrate Properties on Coating's Fragmentation Process. *J. Polym. Sci., Part B: Polymer Physics* **35** (1997) 1449–1461.

46. Y. Leterrier, J. Andersons, Y. Pitton, and J.-A. E. Manson, Adhesion of Silicon Oxide Layers on Poly(ethylene terepthalate). II Effect of Coating Thickness on Adhesive and Cohesive Strengths. *J. Polym. Sci., Part B: Polymer Physics* **35** (1997) 1463–1472.
47. A. S. D. Wang and F. W. Crossman, Initiation and Growth of Transverse Cracks and Edge Delamination in Composite Laminates: Part 1. An Energy Method. *J. Comp. Mat Supplement* **14** (1980) 71–106.
48. A. S. D. Wang, Growth Mechanisms of Transverse Cracks and Ply Delamination in Composite Laminates.. *Proc* 3^{rd} *Int'l Conf. on Comp. Mat.* **Paris** (1980) 170–185.
49. F. W. Crossman and A. S. D. Wang, The Dependence of Transverse Cracking and Delamination on Ply Thickness in Graphite/Epoxy Laminates. *ASTM STP* **775** (1982) 118–139.
50. T. K. O'Brien, Analysis of Local Delaminations and Their Influence on Composite Behavior. In *ASTM STP 876*, ed., W. S. Johnson, in Delamination and Debonding of Materials (1985) 282–297.
51. A. S. D. Wang, N. N. Kishore and C. A. Li, Crack Development in Graphite-Epoxy Cross-Ply Laminates under Uniaxial Tension. *Comp. Sci. & Tech.* **24** (1985) 1–31.
52. L. R. Dharani and H. Tang, Micromechanics Characterization of Sublaminates Damage. *Int. J. Fracture* **46** (1990) 123–140.
53. S. A. Salpekar and T. K. O'Brien, Analysis of Matrix Cracking and Local Delamination in $(0/\theta/-\theta)_s$ Graphite Epoxy Laminates Under Tension Load. *Proc.* 8^{th} *Int'l Conf. on Comp. Mat.* **28-G** (1991) 1–14.
54. J. A. Nairn and S. Hu, The Initiation and Growth of Delaminations Induced by Matrix Microcracks in Laminated Composites. *Int. J. Fract.* **57** (1992) 1–24.
55. C. T. Herakovich, J. G. Davis, Jr., and J. S. Mills, Thermal microcracking in Celion 6000/PMR-15 Graphite/Polyimide. *Thermal Stresses in Severe Environments* (1980) 649–664.
56. C. T. Herakovich and M. W. Hyer, Damage-Induced Property Changes in Composites Subjected to Cyclic Thermal Loading. *Eng. Fract. Mech.* **25** (1986) 779–791.
57. C. Henaff-Gardin, M. C. Lafarie-Frenot, and J. L. Desmeuzes, Modeling of crack evolution under cyclic thermal loading in cross-ply laminates. *Proc. ICCM-10* **Aug 14-18, 1995, Vancouver, BC, Canada** (1995).
58. C. Hnaff-Gardin, M. C. LaFarie-Frenot, and I. Goupillaud, Prediction of Cracking Evolution Under Uniaxial Fatigue Loading in Cross-Ply Composite Laminates. *8th Int'l Mtg., Int'l Conf. on Fatigue of Composites* **Paris, June 3-5, 1997** (1997).
59. S. Hu, J. S. Bark, and J. A. Nairn, On the Phenomenon of Curved Microcracks in $[(S)/90_n]_s$ Laminates: Their Shapes, Initiation Angles, and Locations. *Comp. Sci. & Tech.* **47** (1993) 321–329.
60. P. A. Smith and S. L. Ogin, On Transverse Matrix Cracking in Cross-Ply Laminates Loaded in Simple Bending. *Composites Part A* **30** (1999) 1003–1008.
61. S. R. Kim and J. A. Nairn, Fracture Mechanics Analysis of Coating/Substrate Systems Subjected to Tension or Bending Loads I: Theory. *Eng. Fract. Mech.* **in press** (2000).
62. S. R. Kim and J. A. Nairn, Fracture Mechanics Analysis of Coating/Substrate Systems Subjected to Tension or Bending Loads I: Experiments in Bending. *Eng. Fract. Mech.* **in press** (2000).
63. L. N. McCartney and C. Pierce, Stress Transfer Mechanics for Multiple Ply Laminates Subject to Bending. *NPL Report CMMT(A)55* (1997).
64. L. N. McCartney and C. Pierce, Stress Transfer Mechanics for Multiple Ply Laminates for Axial Loading and Bending. *Proc. ICCM-11* **Australia** (1997).
65. R. G. Spain, Thermal Microcracking of Carbon Fibre/Resin Composites. *Composites* **2** (1971) 33–37.
66. D. S. Adams, D. E. Bowles, and C. T. Herakovich, Thermally Induced Transverse Cracking in Graphite/Epoxy Cross-Ply Laminates. *J. Reinf. Plast. & Comp.* **5** (1986) 152–169.
67. H. L. McManus, D. E. Bowles, and S. S. Tompkins, Prediction of Thermal Cycling Induced Matrix Cracking. *J. Reinf. Plast. & Comp.* **15** (1996) 124–140.
68. C. H. Park and H. L. McManus, Thermally Induced Damage in Composite Laminates: Predictive Methodology and Experimental Investigation. *Comp. Sci. & Tech.* **56** (1996) 1209–1219.

69. T. G. Reynolds and H. L. McManus, Understanding and Accelerating Environmentally-Induced Degradation and Microcracking. *39th AIAA/ASME/ASCE/AHS/ASC Structures, Structural Dynamics Conf.* **Long Beach, CA, April 1998** (1998) 1–8.
70. H. W. Kim, M. A. Grayson, and J. A. Nairn, The Effect of Hygrothermal Aging on the Microcracking Properties of Some Carbon Fiber/Polyimide Laminates. *Adv. Comp. Letters* **4** (1995) 185–188.
71. J. A. Nairn and M. H. Han, Hygrothermal Aging of Polyimide Matrix Composite Laminates. *Proc. ICCM 12* **Paris** (1999).
72. H. W. Kim, Physical Aging Effects on the Microcracking Toughness in Advanced Composites, Ph.D. Thesis, University of Utah, 1996.
73. M. D. Gilchrist, A. J. Kinloch, F.L. Mathews, and S. O. Osiyemi, Mechanical Performance of Carbon-Fibre- and Glass-Fibre-Reinforced Epoxy I-Beams: I. Mechanical. *Comp. Sci. & Tech.* **56** (1996) 37–53.
74. K. L. Reifsnider, Some Fundamental Aspects of the Fatigue and Fracture Response of Composite Materials. *Proc.* 14^{th} *Annual Meeting of SES, Lehigh, PA, November* **Lehigh, PA, November** (1977) 373–383.
75. R. P. Harrison and M. G. Bader, Damage Development in CFRP Laminates under Monotonic and Cyclic Stressing. *Fibre Sci & Tech.* **18** (1983) 163–180.
76. A. S. D. Wang, P. C. Chou and S. C. Lei, A Stochastic Model for the Growth of Matrix Cracks in Composite Laminates. *J. Comp. Mat.* **18** (1984) 239–254.
77. S. L. Ogin, P. A. Smith, and P. W. R. Beaumont, A Stress Intensity Approach to the Fatigue Growth of Transverse Ply Cracks. *Comp. Sci. & Tech* **24** (1985) 47–59.
78. S. L. Ogin, P. A. Smith, and P. W. R. Beaumont, Matrix Cracking and Stiffness Reduction during the Fatigue of a $(0/90)_s$ GFRP Laminate. *Comp. Sci. & Tech.* **22** (1985) 23–31.
79. S. L. Ogin and P. A. Smith, Fast Fracture and Fatigue Growth of Transverse Ply Cracks in Composite Laminates. *Scripta Met.* **June** (1985) 779–784.
80. S. Liu and J. A. Nairn, Fracture Mechanics Analysis of Composite Microcracking: Experimental Results in Fatigue. *Proc. of the Amer. Soc. of Comp.,* 5^{th} *Tech. Conf.* (1990) 287–295.
81. S. Yalvac, L. D. Yats, and D. G. Wetters, Micromechanical Analysis of Fatigue of Toughnened and Untoughened Graphite/Polycyanate Cross-Ply Laminates. *Proc.* 8^{th} *Int'l Conf. on Comp. Mat.* (1991).
82. L. Boniface, S. L. Ogin, and P. A. Smith, Strain Energy Release rates and the Fatigue Growth of Matrix Cracks in Model Arrays in Composite Laminates. *Proc. R. Soc. Lond. A* **432** (1991) 427–444.
83. X. Diao, L. Ye, and Y.-W. Mai, A Statistical Model of Residual Strength and Fatigue Life of Composite Laminates. *Comp. Sci. & Tech.* **54** (1995) 329–336.
84. J. Tong, F. J. Guild, S. L. Ogin, and P. A. Smith, Off-Axis Fatigue Crack Growth and the Associated Energy Release Rate in Composite Laminates. *Appl. Comp. Mater.* **4** (1997) 349–359.
85. G. P. Fang, R. A. Schapery, and Y. Weitsman, Thermally-Induced Fracture in Composites. *Eng. Fract. Mech.* **33** (1989) 619–632.
86. L. Boniface, S. L. Ogin, and P. A. Smith, The Change in Thermal Expansion Coefficient as a Damage Parameter During Thermal Cycling of Crossply Laminates. *Fourth Symposium on Composite Materials: Fatigue and Fracture* **May 6-7, 1991, Indianapolis, Indiana** (1991).
87. H. T. Hahn and T. Johannesson, Fracture Mechanics of Unidirectional Composites: Theory and Applications. In *Mechanics of Composites*, ed., G. J. Dvorak, AMD-V58, ASME (1983) 135–142.
88. A. S. D. Wang, P. C. Chou and S. C. Lei, A Stochastic Model for the Growth of Matrix Cracks in Composite Laminates. *J. Comp. Mat.* **18** (1984) 239–254.
89. D. L. Flaggs, Prediction of Tensile Matrix Failure in Composite Laminates. *J. Comp. Mat.* **19** (1985) 29–50.
90. J. A. Nairn, The Strain Energy Release Rate of Composite Microcracking: A Variational Approach. *J. Comp. Mat.* **23** (1989) 1106–1129.
91. S. C. Tan and R. J. Nuismer, A Theory for Progressive Matrix Cracking in Composite Laminates. *J. Comp. Mat.* **23** (1989) 1029–1047.
92. J. Varna and L. A. Berglund, A Model for Prediction of the Transverse Cracking Strain in Cross-Ply Laminates. *J. Reinf Plast. and Comp.* **11** (1992) 708–728.

93. L. N. McCartney, The Prediction of Cracking in Biaxially Loaded Cross-Ply Laminates Having Brittle Matrices. *Composites* **24** (1993) 84–92.
94. Z. C. Xia, R. R. Carr, and J. W. Hutchinson, Transverse Cracking in Fiber-Reinforced Brittle Matrix, Cross-Ply Laminates. *Acta Metall. Mater.* **41** (1993) 2365–2376.
95. Z. Hashin, Finite Thermoelastic Fracture Criterion with Application to Laminate Cracking Analysis. *J. Mech. Phys. Solids* **44** (1996) 1129–1145.
96. J. A. Nairn, Exact and Variational Theorems for Fracture Mechanics of Composites with Residual Stresses, Traction-Loaded Cracks, and Imperfect Interfaces. *Int. J. Fract.* **in press** (2000).
97. J. A. Nairn, Applications of Finite Fracture Mechanics for Predicting Fracture Events in Composites. *Fifth Int'l Conf. on Deformation and Fracture of Composites* (1999) 1–10.
98. J. A. Nairn, Liu Y. C., On the Use of Energy Methods for Interpretation of Results of Single-Fiber Fragmentation Experiments. *Composite Interfaces* **4** (1997) 241–267.
99. X.-F. Zhou, Nairn J. A., Wagner, H. D., Fiber-Matrix Adhesion From the Single-Fiber Composite Test: Nucleation of Interfacial Debonding. *Composites* **30** (1999) 1387–1400.
100. Kanninen M. F., Popelar C.H., "Advanced Fracture Mechanics," Oxford University Press (New York), 1985.
101. J. A. Nairn, Some New Variational Mechanics Results on Composite Microcracking. *Proc.* 10^{th} *Int'l Conf. on Comp. Mat.* **I** (1995) 423–430.
102. J. G. Williams, *Fracture Mechanics of Solids*, John Wiley & Sons, New York (1984).
103. Z. Hashin, Analysis of Cracked Laminates: A Variational Approach. *Mech. of Mat.* **4** (1985) 121–136.
104. Z. Hashin, Analysis of Stiffness Reduction of Cracked Cross-Ply Laminates. *Eng. Fract. Mech.* **25** (1986) 771–778.
105. L. N. McCartney, Analytical Models of Stress Transfer in Unidirectional Composites and Cross-Ply Laminates, and Their Application to the Prediction of Matrix/Transverse Cracking. In *Local Mechanics Concepts for Composite Material Systems*, eds., J. N. Reddy and K. L Reifsnider, Proc. IUTAM Symposium, Blacksburg, VA, 1991 (1992) 251–282.
106. L. N. McCartney, Predicting Transverse Crack Formation in Cross-Ply Laminates. *Comp. Sci. & Tech.* **58** (1998) 1069–1081.
107. L. N. McCartney, Model to Predict Effects of Triaxial Loading on Ply Cracking in General Symmetric Laminates. *Comp. Sci. & Tech.* **in press** (1999).
108. L. N. McCartney, Stress Transfer Mechanics for Ply Cracks in General Symmetric Laminates. *NPL Report CMMT(A)50* (1996).
109. J. A. Nairn, Fracture Mechanics of Composites With Residual Thermal Stresses. *J. Applied Mech.* **64** (1997) 804–810.
110. J. Varna, L. A. Berglund, R. Talreja, and A. Jokovic, A Study of the Crack Opening Displacement of Transverse Cracks in Cross Ply Laminates. *International Journal of Damage Mechanics* **2** (1993) 272–289.
111. J. Varna, L. A. Berglund, A. Krasnikovs, and A. Chihalenko, Crack Opening Geometry in Cracked Composite Laminates. *International Journal of Damage Mechanics* **6** (1997) 96–118.
112. J. Varna and A. Krasnikovs, Transverse Cracks in Cross-ply Laminates. Part 2. Stiffness Degradation. *Mechanics of Composite Materials* **34** (1998) 153–170.
113. R. Joffe and J. Varna, Analytical Modeling of Stiffness Reduction in Symmetric and Balanced Laminates due to Cracks in 90° Layers. *Comp. Sci. & Tech* **59** (1999) 1641–1652.
114. J. Varna, N. Akshantala, and R. Talreja, Crack Opening Displacement and the Associated Response of Laminates with Varying Constraints. *International Journal of Damage Mechanics* **8** (1999) 174–193.
115. J. Varna, R. Joffe, N. V. Akshantala, and R. Talreja, Damage in Composite Laminates with Off-Axis Plies. *Comp. Sci. & Tech.* **59** (1999) 2139–2147.
116. V. M. Levin, On the Coefficients of Thermal Expansion in Heterogeneous Materials. *Mechanics of Solids* **2** (1967) 58–61.
117. Z. Hashin, Thermal Expansion Coefficients of Cracked Laminates. *Comp. Sci. & Tech.* **31** (1988) 247–260.

118. J. A. Nairn and P. Zoller, Matrix Solidification and the Resulting Residual Thermal Stresses in Composites. *J. Mat. Sci.* **20** (1985) 355–367.
119. J. A. Nairn and P. Zoller, The Development of Residual Thermal Stresses in Amorphous and Semicrystalline Thermoplastic Matrix Composites. *ASTM STP 937* (1987) 328–341.
120. J. A. Nairn, Transverse Fracture in Unidirectional Graphite/Polysulfone Composites. *J. Comp. Mat.* **21** (1987) 798–808.
121. D. L. Hunston, Composite Interlaminar Fracture: Effect of Matrix Fracture Energy. *Comp. Tech. Rev.* **6** (1984) 176–180.
122. J. A. Nairn *et al.*, unpublished results.
123. N. V. Akshantala and R. Talreja, A Micromechanics Based Model for Predicting Fatigue Life of Composite Laminates. *Mater. Sci. & Engr.* **in press** (1999).
124. S. L. Liu, Microcracking of Cross-Ply Laminates Under Static and Fatigue Loads, Ph.D. Thesis, University of Utah, 1994.
125. P. C. Paris, R. E. Gomez, and W. E. Anderson, A Rational Analytical Theory of Fatigue. *The Trend in Engineering* **13** (1961) 9–14.